

**NEW TUNER CHARACTERIZATION AND GAIN
COMPENSATION TECHNIQUES FOR ON-WAFER MICROWAVE
NOISE MEASUREMENT**

By

Benson Yang, B.Sc.

A thesis submitted to the Department of Electrical and Computer Engineering

In Partial Fulfillment of the Requirements for

the degree of Master of Applied Science

McMaster University

Hamilton, Ontario, Canada

Copyright ©Benson Yang, 2012

Abstract

Accurate characterization of a noisy device starts with an accurate measurement system. Measurement uncertainty and error continues to be a challenging subject as technology advances. The conventional method to noise characterization of on-wafer devices is to determine its noise parameters. To extract the noise parameters of an unpackaged device involves a sophisticated measurement system and calibration procedure. This thesis presents a new automated on-wafer noise measurement system based on Labview 8.5.1 which is used to examine measurement uncertainty for noise parameter extraction. The software program can be used and customized for a wide range of on-wafer noise measurements. This thesis covers the design and operation of the measurement system, which is then used to analyze measurement uncertainty.

Measurement uncertainty can be due to various sources from environmental surroundings to instrument settings and the components of the system itself. In many scenarios, inaccuracies are random and cannot be completely resolved. In this thesis, a new tuner characterization technique that improves source tuner characterization is presented. Additionally, a new gain compensation technique is applied to measured noise powers that attempt to improve noise parameter extraction accuracy is proposed. The tuner characterization technique is evaluated against a current industry solution and the affects of the gain compensation technique is evaluated using a newly developed figure of merit. This research work concludes that a direct noise power correction is valid and necessary to further improve noise parameter accuracy. However, the proposed technique when applied resulted in minimal change to the overall noise parameter data. It is found that that source termination selection and total points used for fitting continue to be the major source of uncertainty for noise parameter accuracy.

Acknowledgements

I would first and foremost like to thank Dr. Chih-Hung Chen for giving me this research opportunity. Without his continual support and guidance over the past 2 years, this research would have not been successful. I also have to thank Dr. Ognian Marinov, the technical staff at the university especially Terry Greenlay and Steve Dudkiewicz at Maury Microwave for all their assistance and advice in setting up the laboratory. I also have to thank Cheryl Gies for helping me get through all the administration policies of the university.

I also want to thank all my friends and classmates for their support over the past 2 years. Special thanks to Ian Lei and Vinod Narayan. Lastly, I have to thank my wife, Wei-Hsing and my family for their encouragement and support during my graduate study.

Table of Contents

Abstract.....	iii
Acknowledgements.....	iv
Table of Contents.....	v
List of Figures.....	1
List of Tables.....	4
Chapter 1 Introduction.....	5
1.1 Thesis Objective.....	6
1.2 Research Contribution.....	6
1.3 Thesis Organization.....	7
Chapter 2 Noise Fundamentals.....	8
2.1 Electronic Noise in Semiconductor Devices.....	8
2.1.1 Thermal Noise.....	9
2.1.2 Shot Noise.....	9
2.1.3 Generation-recombination (G-R) Noise.....	10
2.1.4 Flicker ($1/f$) Noise.....	10
2.2 Concept of Noise Figure.....	11
2.3 Why Noise Parameters?.....	12
2.4 Noisy Two Port Network.....	12
2.5 Noise Parameter Extraction Techniques.....	13
2.5.1 Lane's Method.....	14
2.5.2 Adamian and Uhlir's Method.....	16
2.5.3 Caruso and Sanninos' Method.....	19
2.5.4 O'Callaghan and Mondal Method.....	21
2.5.5 Mitama and Katohs' Method.....	23
2.5.6 Davidson <i>et al.</i> 's method.....	26
2.5.7 Chen <i>et al.</i> 's method.....	28
Chapter 3 Instrumentation and Measurement.....	32
3.1 Noise Figure Analyzer.....	32
3.1.1 Measurement Uncertainty.....	33
3.1.2 Calibration.....	33
3.2 Performance Network Analyzer.....	34

3.2.1 Measurement Uncertainty	35
3.2.2 Calibration.....	36
3.3 Laboratory Setup.....	36
3.4 Noise Measurement System Calibration.....	38
3.4.1 S-Parameter Measurements.....	39
3.4.2 Noise Power Measurement and Noise Parameter Extraction	42
3.5 Software System Validation	42
3.6 New Tuner Characterization Technique	49
Chapter 4 New Gain Compensation Technique.....	58
4.1 Receiver Gain Analysis.....	58
4.2 New Gain Compensation Technique	60
4.2.1 Experimental Results	61
Chapter 5 Conclusion.....	68
5.1 Future Software Upgrades	68
5.2 Possible Future Research Areas.....	69
References.....	70
Appendix A Scattering Parameters.....	73
Appendix B Network Analyzer: Error Correction Model.....	78
Appendix C S Domain to ABCD Domain Conversion Table.....	90
Appendix D Software Operations Manual.....	92

List of Figures

Figure 2-1: Noise Representation in MOSFET.....	8
Figure 2-2: Noisy Two-port Model.....	12
Figure 2-3: Adamian and Uhlir Method Equivalent Circuit Model [8,19].....	16
Figure 2-4: Mitama and Katohs' Error Term Definition [12,19].....	24
Figure 3-1: Network Analyzer System [15].....	35
Figure 3-2: Complete High Frequency Noise Measurement System [14].....	37
Figure 3-3: Front and cross-sectional view of a standard mechanical tuner [50].	38
Figure 3-4: Schematic Diagram of Noise System [14].....	39
Figure 3-5: Output Impedance Path.....	40
Figure 3-6: Source Tuner Characterization and Input Impedance Path.....	41
Figure 3-7: Real part of S_{11} , $\text{Re}(S_{11})$ using proposed and ATS method.	44
Figure 3-8: Imaginary part of S_{11} , $\text{Im}(S_{11})$ using proposed and ATS method.	44
Figure 3-9: Real part of S_{12} , $\text{Re}(S_{12})$ using proposed and ATS method.	45
Figure 3-10: Imaginary part of S_{12} , $\text{Im}(S_{12})$ using proposed and ATS method.	45
Figure 3-11: Real part of S_{21} , $\text{Re}(S_{21})$ using proposed and ATS method.	46
Figure 3-12: Imaginary part of S_{21} , $\text{Im}(S_{21})$ using proposed and ATS method.	46
Figure 3-13: Real part of S_{22} , $\text{Re}(S_{22})$ using proposed and ATS method.	47
Figure 3-14: Imaginary part of S_{22} , $\text{Im}(S_{22})$ using proposed and ATS method.	47
Figure 3-15: Noise power (P_c) measured vs. calculated (cold state) at 5GHz.....	48
Figure 3-16: Noise power (P_h) measured vs. calculated (hot state) at 5GHz.	48
Figure 3-17: Real part of S_{11} , $\text{Re}(S_{11})$ using proposed and ATS method at position (100, 4500, 4500).....	50
Figure 3-18: Imaginary part of S_{11} , $\text{Im}(S_{11})$ using proposed and ATS method at position (100, 4500, 4500).....	50
Figure 3-19: Real part of S_{12} , $\text{Re}(S_{12})$ using proposed and ATS method at position (100, 4500, 4500).....	51
Figure 3-20: Imaginary part of S_{12} , $\text{Im}(S_{12})$ using proposed and ATS method at position (100, 4500, 4500).....	51
Figure 3-21: Real part of S_{21} , $\text{Re}(S_{21})$ using proposed and ATS method at position (100, 4500, 4500).....	52

Figure 3-22: Imaginary part of S_{21} , $\text{Im}(S_{21})$ using proposed and ATS method position at (100, 4500, 4500).	52
Figure 3-23: Real part of S_{22} , $\text{Re}(S_{22})$ using proposed and ATS method at position (100, 4500, 4500).	53
Figure 3-24: Imaginary part of S_{22} , $\text{Im}(S_{22})$ using proposed and ATS method at position (100, 4500, 4500).	53
Figure 3-25: Real part of S_{11} , $\text{Re}(S_{11})$ using proposed and ATS method at (2410, 632, 4500) and (908, 4500, 608) positions for low and high band respectively.	54
Figure 3-26: Imaginary part of S_{11} , $\text{Im}(S_{11})$ using proposed and ATS method at (2410, 632, 4500) and (908, 4500, 608) positions for low and high band respectively.	54
Figure 3-27: Real part of S_{12} , $\text{Re}(S_{12})$ using proposed and ATS method at (2410, 632, 4500) and (908, 4500, 608) positions for low and high band respectively.	55
Figure 3-28: Imaginary part of S_{12} , $\text{Im}(S_{12})$ using proposed and ATS method at (2410, 632, 4500) and (908, 4500, 608) positions for low and high band respectively.	55
Figure 3-29: Real part of S_{21} , $\text{Re}(S_{21})$ using proposed and ATS method at (2410, 632, 4500) and (908, 4500, 608) positions for low and high band respectively.	56
Figure 3-30: Imaginary part of S_{21} , $\text{Im}(S_{21})$ using proposed and ATS method at (2410, 632, 4500) and (908, 4500, 608) positions for low and high band respectively.	56
Figure 3-31: Real part of S_{22} , $\text{Re}(S_{22})$ using proposed and ATS method at (2410, 632, 4500) and (908, 4500, 608) positions for low and high band respectively.	57
Figure 3-32: Imaginary part of S_{22} , $\text{Im}(S_{22})$ using proposed and ATS method at (2410, 632, 4500) and (908, 4500, 608) positions for low and high band respectively.	57
Figure 4-1: Measured Receiver Gain, G_o (linear value) versus Γ_s at 5GHz.	59
Figure 4-2: Measured Receiver Gain, G_o (linear value) versus Γ_s at 25GHz.	59
Figure 4-3: Measured Available Power Gain, G_{avt} (linear value) variation for one source impedance at 5GHz.	62
Figure 4-4: Measured Available Power Gain, G_{avt} (linear value) variation for one source impedance at 25GHz.	63
Figure 4-5: Calculated percentage variation for different source impedances at 5GHz.	63
Figure 4-6: Calculated percentage variation for different source impedances at 25GHz.	64
Figure 4-7: Source Impedance Smith Chart Coverage at 5GHz.	64

Figure 4-8: Comparison of Noise Power (P_c) measured with and without correction and calculated at 5GHz.	65
Figure A-1: S-Parameter Signal Flow Diagram.....	73
Figure A-2 S-Parameter 2 Port Network.....	74
Figure A-3: S-Parameter 2 Port Network with Load Impedance.....	75
Figure A-4: S-Parameter 2 Port Network with Total Voltage and Current	76
Figure A-5: S-Parameter Complete 2 Port Network.....	77
Figure B-1: Forward Error Model [16].....	79
Figure B-2: Reverse Error Model [16].....	79
Figure B-3 Complete Forward Error Signal Flow [16].....	80
Figure B-4 Complete Reverse Error Signal Flow [16]	81
Figure B-5: Series Rule.....	81
Figure B-6: Parallel Rule	81
Figure B-7: Self Loop Rule.....	82
Figure B-8: Splitting Rule.....	82
Figure B-9: Complete Forward Model.....	82
Figure B-10: Error Model simplification after applying series rule.	83
Figure B-11: Error Model simplification after applying series rule.	83
Figure B-12: Error Model simplification after applying self loop rule.....	84
Figure B-13: Error Model simplification after applying series rule.	84
Figure B-14: Error Model simplification after applying parallel rule.	84
Figure B-15: Error Model simplification after applying series rule.....	85
Figure B-16: Error Model simplification after applying self loop rule.....	85
Figure B-17: Error Model simplification after applying series rule.....	85
Figure B-18: S_{11M} and S_{21M} solution after applying self loop rule.....	86
Figure B-19: One Port Error Signal Flow.....	86
Figure D-1: Software System User Interface.....	92

List of Tables

Table 4-1: Figure of Merit for Noise Power Correction Method.	67
Table 4-2: Extracted Noise Parameters and Gain (G_{θ}) of the Receiver in the Calibration Stage for Corrected and Uncorrected (values in brackets) Noise Powers	67
Table B-1: Forward Transmission Error Terms.....	79
Table B-2: Reverse Transmission Error Terms	80

Chapter 1

Introduction

Noise is everywhere and is simply any type of disturbance that alters a desired outcome. In terms of electronics, it is any disturbance that disrupts and/or alters an electrical signal. Noise can be generated in both active and passive devices which can be said to be internal noise. External noise sources are also present whether it is from other electronic travelling signals to environmental surroundings.

To combat noise in electronics is to characterize and model it and then measure it. Noise at the radio frequency levels becomes highly dominant with the down scaling of transistors. Measuring noise from devices packaged or unpackaged is challenging and can involve using sophisticated systems. A typical on-wafer noise measurement system connects many components such as: a noise figure meter, a network analyzer, switches, bias tees, impedance tuners, connection cables and their respective controller units. The device under test (DUT) is placed on a fully equipped probe station with pressure and vacuum to keep the device level and stable. With everything connected two complete signal paths exist: a noise figure measurement path and a scattering (s-) parameter measurement path. Each system component potentially presents its own error and in turn can impact measurement accuracy. The importance of measurement accuracy is obvious as it enables industry to report and compare specifications with confidence and provides designers a benchmark standard to improve on existing devices. Prior to any measurement, it is a standard practice to undergo a system calibration. Generally, a calibration improves noise measurement accuracy tremendously but not completely. This thesis discovers that even within instrumentation setting can exist trades offs that contribute to the overall

uncertainty of noise measurement and noise parameter extraction. This thesis also explores system characterization improvements.

1.1 Thesis Objective

This thesis covers the design and implementation of a new automated on-wafer noise measurement system and examines noise measurement uncertainties from a system level and the impacts it can potentially carry to an actual DUT noise parameter characterization. The software program is built using Labview 8.5.1 and the main goal of the program is to minimize user interaction and maximize accuracy within an acceptable time period. The functionality of the programs includes: a complete system calibration procedure and noise parameter extraction of an on-wafer DUT. This thesis also examines system level measurement uncertainty and attempts to understand its impact on device characterization. This thesis works discovers and proposes a new tuner characterization and gain compensation technique.

1.2 Research Contribution

There are two key research contributions from this work: one is the new tuner characterization technique that improves source tuner characterization and secondly, a new gain compensation technique that is to be applied to measured noise powers. The objective is to minimize the error from the noise figure analyzer. The technique utilizes system characterization data to calculate a correction factor that is applied to measured noise power results. The tuner characterization technique is evaluated by a current industry solution and the gain compensation technique is evaluated by a newly developed figure of merit.

1.3 Thesis Organization

This thesis is organized into 5 chapters. Chapter 1 introduces the topic of noise and noise measurement for on-wafer applications as well as the motivation of researching measurement uncertainty and the contribution of this thesis. Chapter 2 reviews electronic noise, the concept of noise figure, the theory of a noisy two port network and reviews noise parameter and its extraction methods. Chapter 3 discusses the background and operation of the two major instruments used in noise measurement: the Noise Figure Analyzer (NFA) and the Performance Network Analyzer (PNA) and discusses the theory and design of the new noise measurement software application. It also, presents the new tuner characterization technique and its experimental results. Chapter 4 introduces the new gain compensation technique and studies its experimental results. Chapter 5 concludes this thesis and proposes possible future software upgrades and future research topics.

Chapter 2

Noise Fundamentals

Noise is an unavoidable phenomenon that is present in our surroundings and is generated in semiconductor devices. In order to minimize the effects of electronic noise, it is important to first understand its origin. This chapter introduces the topic of noise in microelectronics, the concepts of noise figure, noisy two port network and noise parameters and reviews various noise parameter extraction methods.

2.1 Electronic Noise in Semiconductor Devices

Noise can be thought as any undesired signal that distorts or alters a desired signal. The noise present in a MOSFET is often represented by its spectral density versus frequency as shown in Figure 2-1. At higher frequencies, noise becomes constant with respect to frequency. This thesis focuses on microwave frequencies or the white noise region.

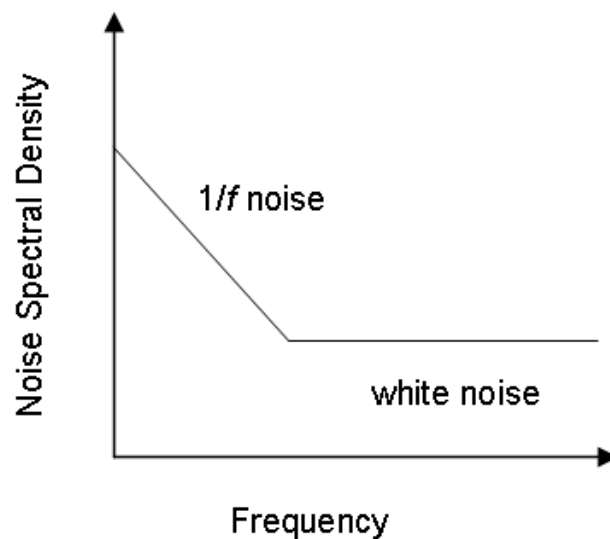


Figure 2-1: Noise Representation in MOSFET.

The most dominant source of electronic noise at microwave frequencies is thermal noise and due to the down scaling of transistor geometry, gate resistance noise increases. Other major sources of electronic noise are shot noise, generation recombination noise and flicker ($1/f$) noise, which are explained the next sections.

2.1.1 Thermal Noise

Thermal noise is produced by the random disruption of charged carriers and atoms in an electrical conductor and can be expressed as a current spectral density [1]

$$S_i = \frac{4k_B T}{R} \quad \text{for} \quad \frac{hf}{kT} \ll 1 \quad (2.1)$$

where f is the frequency, h is Plank's constant, k_B is the Boltzmann constant, T is the absolute lattice temperature and R is the resistance.

At higher frequencies, gate resistance noise is generated by the material of the gate and is expressed by

$$R_g = \frac{R_{gsh} W}{12n_f^2 L} + \frac{\rho_{con}}{WL} \quad (2.2)$$

where R_{gsh} is the gate's sheet resistance, W is the width, L is the length, n_f is the number of fingers and ρ_{con} is the contact resistivity. Clearly, the expression shows that as length decreases, gate noise increases. Therefore, as transistor channel length shorten, this gate noise becomes greater.

2.1.2 Shot Noise

Shot noise is produced by the random emission rate of carriers in an external DC current source and relates to the quantum mechanical direct tunneling process. It can be expressed as a root mean square current fluctuation [1]

$$S_i = 2qI \quad (2.3)$$

where I is the DC current and q is the electronic charge.

2.1.3 Generation-recombination (G-R) Noise

Recombination noise is produced by the random trapping and de-trapping of carriers at any given time which causes fluctuations in the conductance. The current noise density is expressed as [1]

$$S_n = \langle \Delta n^2 \rangle \cdot \frac{4\tau}{1 + (2\pi f \tau_n)^2} \quad (2.4)$$

where Δn^2 is the variance of n , f is the frequency and τ is the lifetime of the carriers.

2.1.4 Flicker (1/f) Noise

Flicker noise occurs at low frequencies and the major cause is unknown. There are three major theories that attempt to describe the origin of this noise. Carrier number fluctuation which explains $1/f$ noise is caused by trapping and de-trapping of charge carriers, mobility fluctuation which attributes $1/f$ noise to photon scattering and an unified model which is an extension of the carrier fluctuation theory that includes Coulomb scattering of free charged carriers. In semiconductors, it is known to have a $1/f$ dependency and is deemed a type of modulation noise. The noise spectral density can be expressed as [2]

$$S_i = \frac{\alpha}{f^n N} \quad (2.5)$$

where α is the Hooge's constant, N is the total number charges and n is a constant close to unity.

2.2 Concept of Noise Figure

The most basic definition according to Friis [3] is, the ratio of the signal to noise power ratio at the input to the signal to noise power ratio at the output and is expressed as

$$F = \frac{S_i/N_i}{S_o/N_o} \quad (2.6)$$

Conventionally, F now refers to the linear value and the noise figure and NF ($10\log(F)$) is the dB value. To understand noise figure measurement it is important to know the relationship between noise temperature and noise figure.

Noise temperature can be thought as the physical temperature of the device. As discussed noise can be a random fluctuation in current due to electron motion in a conductor. When temperature is above absolute zero, the thermal power is directly proportional to the physical temperature and is spread over the entire electromagnetic spectrum. Therefore, thermal noise power is also directly proportional to the bandwidth of the measurement and is expressed as [4]

$$P_N = kTB \quad (2.7)$$

where k is the Boltzmann's constant, T is the ambient temperature and B is the noise bandwidth.

The noise figure is now the figure of merit used to differentiate the noise performance of devices such as amplifiers and electronic systems. The importance of an accurate and repeatable noise measurement system is critical when reporting device noise characteristics. The next chapter will review the key instruments used for microwave noise measurement.

2.3 Why Noise Parameters?

Noise parameters play a critical role in noise characterization of devices. From a practical perspective, measurement systems are typically configured for 50Ω matching. However at the transistor level, this criterion may not produce optimal results. Therefore, with noise parameter information known, a device can be characterized at any impedance by mathematical means. Noise parameters provide a systematic method in determining the optimal noise performance of a device.

2.4 Noisy Two Port Network

The noise of any device is characterized by its noise factor (F) or noise figure (NF) in decibels (dB). This figure of merit was first introduced by Friis [3] and is defined as the ratio of the available signal-to-noise ratio at the input of a two port network to the available signal-to-noise ratio at the output of a two port network at a temperature of 290 Kelvin (K). It can be expressed as in (2.6). A complete definition of s-parameters for a two port network can be found in Appendix A.

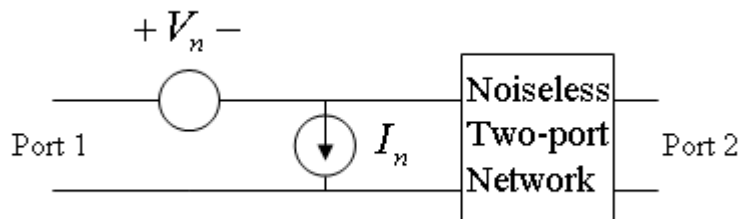


Figure 2-2: Noisy Two-port Model.

A noisy two port network can be modeled by a voltage and a current source as shown in Figure 2-2 with both noise sources being correlated with each other. The noise factor can then be expressed as [6]

$$F = F_{\min} + \frac{R_n}{G_s} \left| Y_s - Y_{\text{opt}} \right|^2 \quad (2.8)$$

where

F_{\min} = the minimum noise factor,

R_n = the equivalent noise resistance, r_n = the normalized noise resistance = R_n/Z_o ,

Z_o = the system characteristic impedance, $Y_o = 1/Z_o$,

Y_s = the source admittance = $G_s + j \cdot B_s$,

Γ_s = the source reflection coefficient = $(Y_o - Y_s)/(Y_o + Y_s)$,

Y_{opt} = the optimal source admittance required to achieve F_{\min} , and

Γ_{opt} = the optimal source reflection coefficient required to achieve F_{\min} .

This noise factor is most commonly obtained by the Y-factor method discussed earlier. Therefore, knowing the noise parameters F_{\min} , R_n , G_s , and B_s , the linear two port noise factor can be calculated for any source admittance.

2.5 Noise Parameter Extraction Techniques

Using the Y-factor method involves experimental data, which introduce possible measurement errors and/or uncertainties when measuring noise power and source admittance. Many noise parameter extraction techniques have been proposed and this section reviews the different methods that attempt to minimize the impacts of experimental errors.

2.5.1 Lane's Method

Theoretically, only four noise measurements are required to solve for the four noise parameters. However, the impact of error is very high when using such a small data set. Lane's method is the considered the fundamental approach of which many newer methods is based upon. It uses mathematically averaging to solve for the noise parameters. The method first re-arranges the noise factor equation in (2.8) to the form [7]

$$F = A + G_s \cdot B + \frac{C + B_s^2 \cdot B + B_s \cdot D}{G_s} \quad (2.9)$$

where

$$F_{\min} = A + \sqrt{4BC - D^2}, \quad (2.10)$$

$$R_n = B, \quad (2.11)$$

$$G_{\text{opt}} = \frac{\sqrt{4BC - D^2}}{2B}, \quad (2.12)$$

and

$$B_{\text{opt}} = -\frac{D}{2B}. \quad (2.13)$$

Since, the noise factor (F) is a measured value. There are potential errors as discussed in later in this thesis. Lane proposes the use of a least-squares fit approach to solving for A , B , C and D .

This method first defines an error term given by

$$\mathcal{E} \equiv \frac{1}{2} \sum_{i=1}^n w_i \cdot \left[A + \left(G_{si} + \frac{B_{si}^2}{G_{si}} \right) \cdot B + \frac{1}{G_{si}} \cdot C + \frac{B_{si}}{G_{si}} \cdot D - F_i^m \right]^2 \quad (2.14)$$

where

i is the i^{th} data point,

F_i^m is the measured noise factor at i^{th} point,

w_i is the weighting factor at the i^{th} point,

G_{si} is the real part of the source admittance Y_s ,

B_{si} is the imaginary part of the source admittance Y_s and

ε is the error between the fitted noise factor and the measured noise factor.

The weighting factor in practice is typically set to one, which means it is generally not used.

Also, Lane does not propose any methods to obtain a suitable value for this variable. To minimize ε , the first order derivative is taken with respect to A , B , C and D and set to zero.

Therefore, the following equations can be obtained

$$\frac{\partial \varepsilon}{\partial A} = \sum_{i=1}^n W_i P = 0, \quad (2.15)$$

$$\frac{\partial \varepsilon}{\partial B} = \sum_{i=1}^n W_i \left(G_i + \frac{B_i^2}{G_i} \right) P = 0, \quad (2.16)$$

$$\frac{\partial \varepsilon}{\partial C} = \sum_{i=1}^n W_i \left(\frac{P}{G_i} \right) = 0, \quad (2.17)$$

$$\frac{\partial \varepsilon}{\partial D} = \sum_{i=1}^n W_i \left(\frac{B_i}{G_i} \right) P = 0, \quad (2.18)$$

where $P = \left[A + B \left(G_i + \frac{B_i^2}{G_i} \right) + \frac{C}{G_i} + \frac{DB_i}{G_i} - F_i \right]$.

Lane's method makes the assumption that the source of error occurs only in the noise power measurement and not in the source admittance. This assumption is later discovered to be incorrect and will be discussed in later methods. It also is very dependent on B (or R_n), as B_{opt} and G_{opt} approach zero for large R_n devices. Nonetheless, Lane's method still formed the basis for noise parameter extraction and is the $ABCD$ extraction method used in this thesis.

2.5.2 Adamian and Uhlir's Method

Adamian and Uhlir proposes a method that uses measured noise powers at various source admittances to characterize a noisy receiver. Figure 2-3 shows the equivalent circuit model of the receiver which has a voltage source and a current source that are correlated [8].

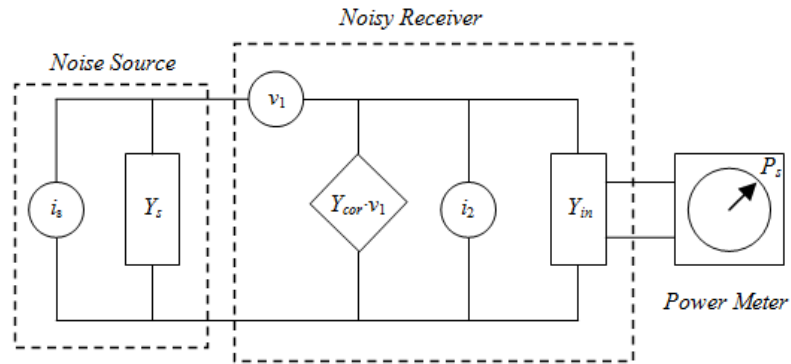


Figure 2-3: Adamian and Uhlir Method Equivalent Circuit Model [8,19].

Based on the model, the received noise power is given by [8]

$$P_s = \frac{4kT_o K G_{in}}{|Y_s + Y_{in}|^2} (|Y_s + Y_{cor}|^2 \cdot R_n + G_n + t_s G_s) \quad (2.19)$$

where

$$R_n = \frac{\overline{|v_1|^2}}{4kT_o\Delta f}, \quad (2.20)$$

$$G_n = \frac{\overline{|i_2|^2}}{4kT_o\Delta f}, \quad (2.21)$$

and

$$t_s = \frac{T_s}{T_o}. \quad (2.22)$$

The following list defines the rest of the variables,

Y_s is the output admittance of the noise source,

Y_{in} is the input admittance of the receiver,

i_s is the current source,

v_1 is the voltage source,

$Y_{cor \cdot v_1}$ is the correlated part of the noise source,

k is Boltzmann's constant,

T_o is the standard temperature 290K,

T_s is the noise temperature of the source,

K is an arbitrary constant,

Δf is the noise bandwidth,

G_{in} is the real part of Y_{in} and

B_{in} is the imaginary part of Y_{in} .

To solve for the noise parameters, K must first be obtained through a unique test case where the source admittances under hot and cold states are assumed to be equal (ie. $Y_{sc} = Y_{sh}$). By taking hot and cold noise power measurements, K can be solved by

$$K = \frac{(P_{sh} - P_{sc}) |Y_{in} + Y_s|^2}{4kT_o \Delta f G_{in} (t_{sh} - t_{sc})} \quad (2.23)$$

where

P_{sh} is the noise power in the hot state,

P_{sc} is the noise power in the cold state,

t_{sh} is the normalized noise temperature in the hot state and

t_{sc} is the normalized noise temperature in the cold state.

Then, the A , B , C and D can be solved using the least-square fit method by re-arranging the (2.23) into the form

$$\lambda P_s |Y_s + Y_{in}|^2 - t_s G_s = |Y_s|^2 \cdot A + B + 2G_s \cdot C + 2B_s \cdot D \quad (2.24)$$

where

$$\lambda = \frac{1}{4kT_o \Delta f K G_{in}}, \quad (2.25)$$

$$A = R_n, \quad (2.26)$$

$$B = G_n + |Y_{cor}|^2 \cdot R_n, \quad (2.27)$$

$$C = G_{cor} \cdot R_n, \quad (2.28)$$

and

$$D = B_{cor} \cdot R_n. \quad (2.29)$$

Once the A , B , C and D are found, the noise parameters can be calculated by

$$F_{min} = 1 + 2R_n G_{cor} + 2\sqrt{R_n G_n + (R_n G_{cor})^2}, \quad (2.30)$$

$$G_{\text{opt}} = \sqrt{\frac{G_n}{R_n} + G_{\text{cor}}^2}, \quad (2.31)$$

$$B_{\text{opt}} = -B_{\text{cor}}, \quad (2.32)$$

where

$$R_n = A, \quad (2.33)$$

$$G_{\text{cor}} = \frac{C}{A}, \quad (2.34)$$

$$B_{\text{cor}} = \frac{D}{A}, \quad (2.35)$$

and

$$G_n = B - |G_{\text{cor}} + j \cdot B_{\text{cor}}|^2 R_n. \quad (2.36)$$

Similarly, with Lane's method, it assumes that the source admittances are equal in hot and cold states. Also, the K is assumed to be constant which in later methods is discovered that this assumption is not correct.

2.5.3 Caruso and Sanninos' Method

Caruso and Sanninos propose a method that uses the effective noise temperatures to solve for the noise parameters which are given by [9]

$$T_e = T_0 \cdot (F - 1), \quad (2.37)$$

$$T_{\text{min}} = T_0 \cdot (F_{\text{min}} - 1). \quad (2.38)$$

The modified noise factor based on Lange work [10] is used and defined as

$$F = F_{\min} + N \frac{|Y_s - Y_{\text{opt}}|^2}{G_{\text{opt}} G_s} \quad (2.39)$$

where

$$N = R_n \cdot G_{\text{opt}}, \quad (2.40)$$

and G_{opt} is the real part of Y_{opt} .

By substituting $Y_s = \frac{1-\Gamma_s}{1+\Gamma_s} \cdot Y_o$, $Y_{\text{opt}} = \frac{1-\Gamma_{\text{opt}}}{1+\Gamma_{\text{opt}}} \cdot Y_o$, (2.37) and (2.38) into (2.39) the following

expression can be derived

$$T_e = T_{\min} + 4T_o N \frac{|\Gamma_s - \Gamma_{\text{opt}}|^2}{(1-|\Gamma_s|^2)(1-|\Gamma_{\text{opt}}|^2)}, \quad (2.41)$$

where

$$\Gamma_s = \rho_s \exp(j\theta_s), \quad (2.42)$$

and

$$\Gamma_{\text{opt}} = \rho_{\text{opt}} \exp(j\theta_{\text{opt}}). \quad (2.43)$$

Then by replacing Γ_s and Γ_{opt} , it can be shown that

$$T_e = A + \frac{1}{1-\rho_s^2} \cdot B + \frac{\rho_s \cos(\theta_s)}{1-\rho_s^2} \cdot C + \frac{\rho_s \sin(\theta_s)}{1-\rho_s^2} \cdot D \quad (2.44)$$

where

$$T_{\min} = A + \frac{B+\Delta}{2}, \quad (2.45)$$

$$N = \frac{\Delta}{4T_o}, \quad (2.46)$$

$$\rho_{\text{opt}} = \sqrt{\frac{B - \Delta}{B + \Delta}}, \text{ where } \Delta = \sqrt{B^2 - C^2 - D^2} \quad (2.47)$$

and

$$\theta_{\text{opt}} = \tan^{-1}\left(\frac{D}{C}\right). \quad (2.48)$$

A , B , C and D can now be solved by applying a least-square fit approach. Caruso and Sanninos found that for particular source admittances (Γ_s) would cause errors in the noise parameter calculations. This observation will be confirmed in later methods as well.

2.5.4 O'Callaghan and Mondal Method

O'Callaghan and Mondal propose a vector based approach to noise parameter extraction from measurement data. The fundamental noise factor equation is re-arranged into the form [11]

$$F = (F_{\text{min}} - 2R_n G_{\text{opt}}) + R_n \left(\frac{G_s^2 + B_s^2}{G_s}\right) - 2R_n B_{\text{opt}} \left(\frac{B_s}{G_s}\right) + R_n (G_{\text{opt}}^2 + B_{\text{opt}}^2) \left(\frac{1}{G_s}\right). \quad (2.49)$$

The equation is divided into four terms each having a different dependence on the source admittance. Then, from each term the following vectors can be defined for n data points as

$$\overline{F}_n^m = (F_1^m, F_2^m, \dots, F_i^m, \dots, F_n^m)^T, \quad (2.50)$$

$$\overline{V}_1 = (1, 1, \dots, 1, \dots, 1)^T, \quad (2.51)$$

$$\overline{V}_2 = \left(\frac{G_{s1}^2 + B_{s1}^2}{G_{s1}}, \frac{G_{s2}^2 + B_{s2}^2}{G_{s2}}, \dots, \frac{G_{si}^2 + B_{si}^2}{G_{si}}, \dots, \frac{G_{sn}^2 + B_{sn}^2}{G_{sn}}\right)^T, \quad (2.52)$$

$$\overline{V}_3 = \left(\frac{B_{s1}}{G_{s1}}, \frac{B_{s2}}{G_{s2}}, \dots, \frac{B_{si}}{G_{si}}, \dots, \frac{B_{sn}}{G_{sn}}\right)^T, \quad (2.53)$$

$$\bar{V}_4 = \left(\frac{1}{G_{s1}}, \frac{1}{G_{s2}}, \dots, \frac{1}{G_{si}}, \dots, \frac{1}{G_{sn}} \right)^T, \quad (2.54)$$

where

F_m^i is the i^{th} measured noise factor,

G_{si} is the i^{th} measured source conductance and

B_{si} is the i^{th} measured source susceptance.

By re-organizing the noise factor equation (2.49) into

$$\bar{F}_n^m = C_1 \bar{V}_1 + C_2 \bar{V}_2 + C_3 \bar{V}_3 + C_4 \bar{V}_4 \quad (2.55)$$

where

$$C_1 = F_{\min} - 2R_n G_{\text{opt}}, \quad (2.56)$$

$$C_2 = R_n, \quad (2.57)$$

$$C_3 = -2R_n B_{\text{opt}}, \quad (2.58)$$

and

$$C_4 = R_n (G_{\text{opt}}^2 + B_{\text{opt}}^2). \quad (2.59)$$

Then, defining an error vector as

$$\bar{E}_{F_n^m} = \bar{F}_n^m - \sum_{j=1}^4 C_j \bar{V}_j. \quad (2.60)$$

Now, applying the Hilbert theorem which states the magnitude of the error vector is minimum when such a vector is orthogonal to all vectors (ie. $\langle \bar{E}_{F_n^m}, \bar{V}_i \rangle = 0$). Using this theorem, the error vector can be expressed as

$$\sum_{j=1}^4 \langle \bar{V}_i, \bar{V}_j \rangle C_j = \langle \bar{F}_n^m, \bar{V}_i \rangle, \quad i = 1, 2, 3, \text{ and } 4 \quad (2.61)$$

The noise parameters can be extracted by applying linear algebra and are given by

$$R_n = C_2, \quad (2.62)$$

$$B_{\text{opt}} = -C_3 / 2R_n, \quad (2.63)$$

$$G_{\text{opt}} = \sqrt{\frac{C_4}{R_n} - B_{\text{opt}}^2}, \quad (2.64)$$

$$F_{\text{min}} = C_1 + 2R_n G_{\text{opt}}. \quad (2.65)$$

The key advantage of this approach is that it presents a method of selecting source admittance points that results in improved noise parameter extraction accuracy.

2.5.5 Mitama and Katohs' Method

Mitama and Katohs' propose an improved method that defines a new error term which includes the possible measurement error in source admittance and is defined as [12]

$$\varepsilon_{ni} = \sqrt{w_{gi} \cdot (G_{si} - G_{si}^m)^2 + w_{bi} \cdot (B_{si} - B_{si}^m)^2 + w_{fi} \cdot (F_i - F_i^m)^2} \quad (2.66)$$

where w_{gi} , w_{bi} , and w_{fi} are the weighting factors for the error term in G_{si} , B_{si} , and F_i , respectively. As shown in the defined error term, both measured uncertainty in the noise factor and source admittance are considered and corrected for.

Mitama and Katohs first assumes $w_{gi} = w_{bi} = w_{fi} = 1$. As shown in Figure 2-4, the minimum value for ε_{ni} occurs when a line is projected from the measured point labeled as $(G_{si}^m, B_{si}^m, F_i^m)$ that is normal to the quasi-elliptic paraboloid.

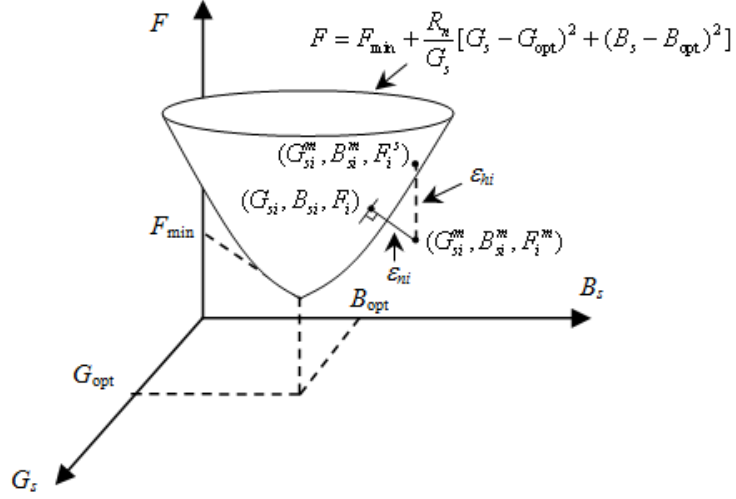


Figure 2-4: Mitama and Katohs' Error Term Definition [12,19].

The error term $\epsilon_{ni_{\min}}$ represents the length between the two points. The next step is to define

$\epsilon_{ni_{\min}}$ and apply the fitting to the sum of all the errors that is given by

$$S = \min\left(\sum_{i=1}^n \epsilon_{ni_{\min}}^2\right). \quad (2.67)$$

First an error function is defined as

$$\hat{F}(G_s, B_s, F_m, F_{\min}, R_n, G_{opt}, B_{opt}) = F_{\min} + \frac{R_n}{G_s} \left[(G_s - G_{opt})^2 + (B_s - B_{opt})^2 \right] - F^m \quad (2.68)$$

where F^m is the measured noise factor.

Assuming, $\hat{F}(G_s, B_s, F_m, F_{\min}, R_n, G_{opt}, B_{opt}) \approx 0$, the function can be expanded in a Taylor series

to a first-order approximation as

$$\begin{aligned} & \hat{F}_i^k + \hat{F}_{G_{si}}^k (G_{si} - G_{si}^m) + \hat{F}_{B_{si}}^k (B_{si} - B_{si}^m) + \hat{F}_{F_{si}^m}^k (F_i - F_i^m) \\ & + \hat{F}_{F_{\min}^m}^k (F_{\min} - F_{\min}^m) + \hat{F}_{R_n}^k (R_n - R_n^k) + \hat{F}_{G_{opt}^k}^k (G_{opt} - G_{opt}^k) + \hat{F}_{B_{opt}^k}^k (B_{opt} - B_{opt}^k) = 0 \end{aligned} \quad (2.69)$$

where

\hat{F}_V^k is the partial derivative of the error function with respect to V and V is equal to

$G_s, B_s, F_m, F_{\min}, R_n, G_{opt}$ or B_{opt} ,

k is the k^{th} iteration and can be equal to 0, 1, 2, 3, ... n and

i is the i^{th} measurement point..

Substituting the Taylor series back into the error function (2.68), it yields

$$\mathcal{E}_{ni_{\min}}^k = \sqrt{w_i^k} \cdot |d_i^k| \quad (2.70)$$

where

$$w_i^k = \frac{1}{\frac{\hat{F}_{G,i}^k}{w_{gi}} + \frac{\hat{F}_{B,i}^k}{w_{bi}} + \frac{\hat{F}_{F^m,i}^k}{w_{fi}}} \quad (2.71)$$

and

$$d_i^k = -\left[\hat{F}_i^k + \hat{F}_{F_{\min},i}^k (F_{\min} - F_{\min}^k) + \hat{F}_{R_n,i}^k (R_n - R_n^k) + \hat{F}_{G_{opt},i}^k (G_{opt} - G_{opt}^k) + \hat{F}_{B_{opt},i}^k (B_{opt} - B_{opt}^k) \right]. \quad (2.72)$$

By applying the least-square fit to solve the following linear equations

$$\frac{\partial \mathcal{S}}{\partial F_{\min}} = 2 \sum_{i=1}^n w_i \hat{F}_{F_{\min},i}^k d_i^k = 0, \quad (2.73)$$

$$\frac{\partial \mathcal{S}}{\partial R_n} = 2 \sum_{i=1}^n w_i \hat{F}_{R_n,i}^k d_i^k = 0, \quad (2.74)$$

$$\frac{\partial \mathcal{S}}{\partial G_{opt}} = 2 \sum_{i=1}^n w_i \hat{F}_{G_{opt},i}^k d_i^k = 0, \quad (2.75)$$

$$\frac{\partial \mathcal{S}}{\partial B_{opt}} = 2 \sum_{i=1}^n w_i \hat{F}_{B_{opt},i}^k d_i^k = 0. \quad (2.76)$$

To solve the linear equations, the conventional least-squares fit method (ie. Lane's Method) must be applied first to determine the initial values of F_{\min}^0 , R_n^0 , G_{opt}^0 , and B_{opt}^0 . The key improvement of Mitama and Katoh's method is that it factors in the uncertainty in source admittance and noise factor. This contribution later became the basis for new research and improvements which are discussed in the upcoming sections.

2.5.6 Davidson *et al.*'s method

Davidson *et al.* propose a method to noise parameter extraction that uses noise power measurements to improve extraction accuracy and it also minimizes the impact of different source impedances in hot and cold states. First, assuming the hot and cold source impedances to be equal, the difference between hot and cold noise power can be expressed by [13]

$$P_h - P_c = k(T_h - T_c)\Delta f \frac{1 - |\Gamma_s|^2}{|1 - \Gamma_s \Gamma_l|^2} G_o \quad (2.77)$$

where

k is Boltzmann's constant,

T_h is the noise temperature of the source in the hot state,

T_c is the noise temperature of the source in the cold state,

G_o is an unknown constant,

Γ_s is the reflection coefficient at the source and

Γ_l is the reflection coefficient at the load.

The standard noise factor equation, $F = \frac{ENR}{Y-1}$, can be simplified when ambient temperature (T_c) is equal to T_0 (290K) to

$$F = \frac{ENR}{Y-1} = \frac{ENR \cdot P_c}{P_h - P_c}. \quad (2.78)$$

After substitution, the noise factor becomes

$$F = \frac{ENR}{k(T_h - T_c)\Delta f G_o} \cdot \frac{P_c}{g_s} = \frac{1}{m} \cdot \frac{P_c}{g_s}, \quad (2.79)$$

where $g_s = \frac{1 - |\Gamma_s|^2}{|1 - \Gamma_s \Gamma_l|^2}$ and m is a unknown constant.

Using $F = F_{\min} + \frac{R_n}{G_s} |Y_s - Y_{\text{opt}}|^2$ and (2.79), the following equation is derived

$$\frac{P_c}{g_s} = mF = mF_{\min} + \frac{mR_n}{G_s} |Y_s - Y_{\text{opt}}|^2. \quad (2.80)$$

From applying the least-squares fit approach to (2.80), the noise parameters extracted are: mF_{\min} , mR_n , G_{opt} , and B_{opt} . Now, the constant m , must be determined and by combining (2.80) and (2.78), it becomes

$$m = \frac{P_h^m - P_c^c}{ENR \cdot g_{sh}} \quad (2.81)$$

where

g_{sh} is the calculated result from (x) in the hot state,

P_c^c is the calculated cold noise power from (y) and

P_h^m is the measured noise power in the hot state.

Once m is known, the final F_{\min} and R_n are calculated. This method although improves noise parameter accuracy by minimizing the impact from different hot and cold source impedances, it also makes key assumptions that introduce uncertainty to its method (ie. $T_c = T_0$).

2.5.7 Chen *et al.*'s method

Chen *et al.* proposes a method that based on noise power measurements and further improves noise parameter extraction accuracy by accounting for the impacts of source impedances and noise temperatures in hot and cold states. The noise power can be expressed by [14]

$$P_n = \frac{G_{tr}}{4R_s} \left[4kT_{seff} \Delta f R_s + |\bar{i}_{in}|^2 |Z_s|^2 + |\bar{u}|^2 (1 + |Y_{cor}|^2 |Z_s|^2 + 2G_{cor} R_s - 2B_{cor} X_s) \right] \quad (2.82)$$

where

k is the Boltzmann constant,

T_0 is the standard temperature (= 290K),

Δf is the noise bandwidth,

R_s is the source resistance,

X_s is the source reactance,

Z_s is the source impedance,

\bar{u} is the referred noise voltage,

\bar{i}_{in} is the input referred noise current,

G_{cor} is the correlation conductance,

B_{cor} is the correlation susceptance,

Y_{cor} is the complex correlation admittance,

G_{tr} is the transducer power gain of the receiver and

T_{seff} is the effective source temperature.

Re-arranging (2.82), the noise power expression becomes

$$\frac{P_n G_s}{kT_0 \Delta f} \cdot \frac{|1 - \Gamma_{inr} \Gamma_s|^2}{1 - |\Gamma_s|^2} = (T_{seffnor} G_s + |Y_s|^2 A + B + 2G_s C + 2B_s D) G_0, \quad (2.83)$$

where

P_n is the noise power in either hot or cold state,

G_0 is the receiver gain,

$T_{seffnor}$ is the normalized effective source temperature,

Y_s is the source admittance,

G_s is the source conductance,

B_s is the source susceptance,

Γ_{inr} is the input reflection coefficient of the receiver,

Γ_s is the source reflection coefficient,

A is a noise parameter coefficient,

B is a noise parameter coefficient,

C is a noise parameter coefficient and

D is a noise parameter coefficient.

Before apply the least-squares fit approach to solve for A , B , C , and D . G_0 is calculated by setting $A=B=C=D=0$ and by taking into account the hot and cold state difference in noise temperature, source admittance and noise power, (2.83) becomes

$$G_0 = \frac{1}{kT_0\Delta f(T_{seffnorh}G_{sh} - T_{seffnorc}G_{sc})} \left(P_h G_{sh} \frac{|1 - \Gamma_{inv}\Gamma_{sh}|^2}{1 - |\Gamma_{sh}|^2} - P_c G_{sc} \frac{|1 - \Gamma_{inv}\Gamma_{sc}|^2}{1 - |\Gamma_{sc}|^2} \right). \quad (2.84)$$

Substituting the calculated G_0 back into (2.83) and applying a fitting method, the A , B , C and D noise parameters can be extracted and the actual noise parameters can be determined using

$$R_u = A, \quad (2.85)$$

$$G_{iun} = B - \frac{C^2 + D^2}{A}, \quad (2.86)$$

$$G_{cor} = \frac{C}{A}, \quad (2.87)$$

$$B_{cor} = \frac{D}{A}, \quad (2.88)$$

$$NF_{\min} = 1 + 2R_u G_{cor} + 2\sqrt{R_u G_{iun} + (R_u G_{cor})^2}, \quad (2.89)$$

$$R_n = R_u, \quad (2.90)$$

$$G_{opt} = \sqrt{\frac{G_{iun}}{R_u} + G_{cor}^2}, \quad (2.91)$$

$$B_{opt} = -B_{cor}. \quad (2.92)$$

Chen *et al.*'s method builds upon past techniques and further improves noise parameter accuracy by simultaneously addressing error in source admittance and noise temperature. However, it does not address measurement error from instrumentation (ie. the noise figure analyzer). This thesis proposes a gain compensation technique that can be applied to the noise power measurement data directly.

Chapter 3

Instrumentation and Measurement

The topics of instrumentation and measurement are both essential to device characterization as quality measurements are only as accurate as what is reported by the instrument. This chapter provides an overview of the two key instruments used in noise measurement, introduces the subject of measurement uncertainty from an instrumentation perspective and reviews the measurement system and experimental results of this thesis.

3.1 Noise Figure Analyzer

Noise characterization of the measurement system is a crucial step as noise introduced by the system can impact DUT noise characterization accuracy. The NFA is the standard instrument used for noise figure measurement. A typical NFA consists of a receiver with an accurate power detector and circuitry to control a noise source. The most accepted method to compute the noise figure is the Y-factor method. This method requires a pre-calibrated noise source with a known excess noise ratio (ENR) table. ENR can be defined as [4]

$$ENR = \frac{(T_s^{ON} - T_s^{OFF})}{T_0} \quad (3.1)$$

where T_s^{ON} and T_s^{OFF} are the noise temperatures of the noise source in its ON/OFF states.

This calibration information is loaded into the NFA and is used by the instrument for noise property determination. The Y-factor is the ratio of the power level with noise source ON and power level with noise source OFF and is given by [4]

$$Y = \frac{N^{ON}}{N^{OFF}}. \quad (3.2)$$

Lastly, the noise factor (F) is proportional to ENR and the Y-factor and can be expressed as [4]

$$F = \frac{ENR}{Y - 1}. \quad (3.3)$$

3.1.1 Measurement Uncertainty

The NFA is manufactured to be an accurate power meter and based on [5] it was found that the power detector mechanism within the instrument can cause measurement error in two forms:

- power absorption within the mount
- uneven current distribution

Also, when making a measurement, the NFA assumes that the DUT has an amplitude versus frequency characteristics that is constant over the IF bandwidth [4]. Later, it is observed that the system characteristics are not constant within this bandwidth which makes this assumption false and results in additional measurement uncertainty.

3.1.2 Calibration

The NFA also is built with a self-calibration mechanism that conventionally uses a noise source with a known ENR table that becomes the benchmark reference when measuring the noise figure of a DUT. For the purpose of this thesis, the NFA is solely used as a power meter and a self-calibration is not required.

3.2 Performance Network Analyzer

The basic signal flow of a standard network analyzer (NA) is shown in Figure 3-1. During measurement, the source supplies the incident signal to the DUT and can sweep a range of frequencies based on the manufacturer's specifications. When the incident signal reaches the DUT, part of the signal is reflected due to mismatch and the remaining signal is transmitted through the DUT. At the signal processing stage, the three signals are separated and the information is processed. The information of each signal is passed to the receiver/detector stage where each signal is measured and compared. The information at this stage is also converted into displayable digital information. Finally, all the computation and reflection and transmission information is processed and displayed at the processor/display stage. The reflection measurements are determined by comparing the incident and reflected signal. The DUT reflection characteristics such as return loss, standing wave ratio, reflection coefficients (for example, S_{11}) and impedance are then returned and/or displayed. The transmission measurements are determined by comparing the incident and transmitted signal. The DUT transmission characteristics such as insertion loss, electrical delay, transmission coefficients (for example, S_{21}) and phase and group delay are then returned and/or displayed. The NA also can determine the reverse characteristics such as, S_{22} , S_{12} and output impedance. S-parameter definitions are reviewed in Appendix A.

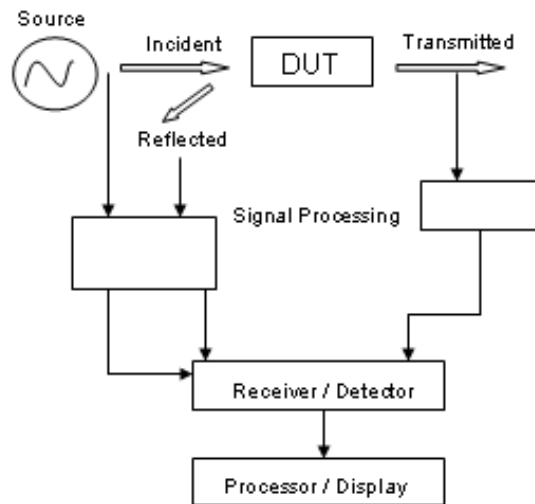


Figure 3-1: Network Analyzer System [15].

3.2.1 Measurement Uncertainty

Measurement accuracy is very important for device characterization, as errors can impact measurement results. The network analyzer can be calibrated a number of ways depending on what is being tested and how accurate a particular measurement needs to be. There are three main types of errors that contribute to measurement error which are:

1. Systematic error, which is caused by system setup issues and equipment
2. Random error, which is caused by intermittent noise (for example, source phase noise and IF noise)
3. Drift error, which is caused by environmental changes after calibration (for example, temperature)

Random and drift error cannot be removed by instrument calibration as its effects are caused by nature and its surroundings. Systematic errors can be categorized into three groups and are due

to: Leakage, Reflection and Frequency Response Differences. Calibration techniques therefore only address systematic errors. Therefore, even after a successful calibration, there are still possible errors that can arise during measurement that cannot be resolved and are random in nature.

3.2.2 Calibration

The calibration process discussed in this section is for a conventional two port NA. A two port NA can be calibrated at any single port or can undergo a full two-port calibration. For a one port calibration, a known open, short and load standard is connected to the desired port. Using the known standard information the NA can move the measurement reference plane from the instrument to the input connection of each standard for accurate DUT measurement. In order to move the reference plane, the NA calculates three error terms during the calibration stage and will remove their contribution when measuring the DUT. A full two port calibration can be performed via the Thru, Reflect and Line (TRL) method or Short, Open, Load and Thru (SOLT) method. Each method will determine the twelve error terms required to remove all systematic measurement errors. Appendix B reviews the complete details and derivations of the error terms. SOLT involves obtaining the one port errors terms using the short, open, load standards at port one and two, the transmission tracking error terms using the thru standard and isolation error terms using the load standard. The SOLT calibration method was used in this thesis.

3.3 Laboratory Setup

The complete system for high frequency noise measurement is shown in Figure 3-2.

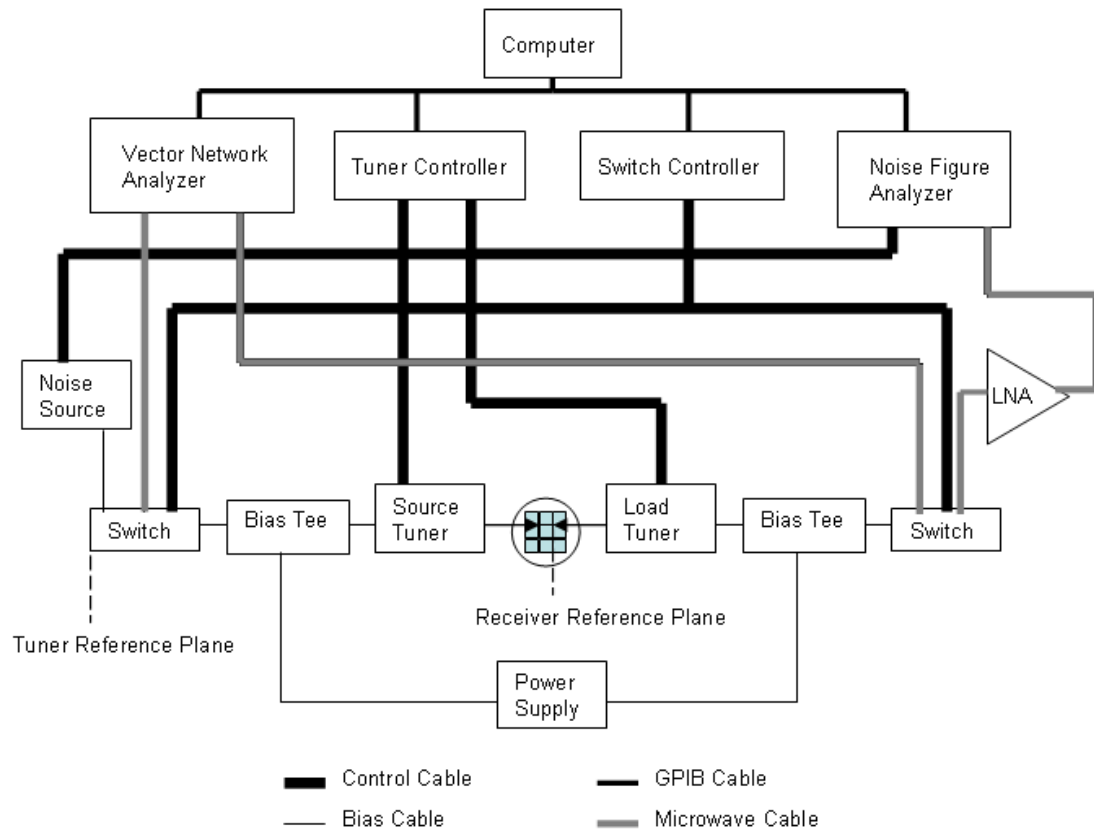


Figure 3-2: Complete High Frequency Noise Measurement System [14].

The system consists of a desktop computer which is connected to an Agilent Performance Network Analyzer N5230A (PNA), an Agilent Noise Figure Analyzer N8975A (NFA), a Maury Microwave Automated System Controller, an Agilent Switch Controller and a Hewlett Packard DC Power Supply via a General Purpose Interface Bus (GPIB) connection. The system is connected in such a way that there exist two measurement paths, a noise path and s-parameter path. By controlling the switch, an active path can be set. For the noise path, the NFA is connected to a noise source which passes through a bias tee, which is used to provide the appropriate DC power to the DUT, a controllable Maury Microwave Tuner (source tuner), an on-wafer DUT or calibration substrate, another Maury Microwave Tuner (load tuner), another bias

tee, a low noise amplifier (LNA) and back to the NFA. Similarly, the s-parameter path when set active has the PNA port 1 connected to the bias tee, source tuner, the DUT or calibration substrate, the load tuner, bias tee and back to the PNA port 2.

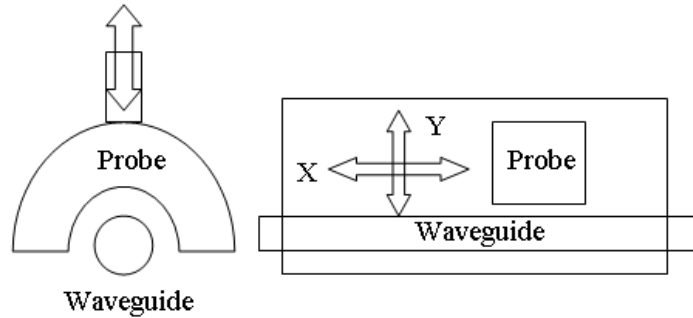


Figure 3-3: Front and cross-sectional view of a standard mechanical tuner [50].

The Maury Microwave source tuner is tuned by setting the probe's x and y coordinates and supports frequencies between 4 and 26.5GHz. The default position is set at (100,4500,4500), which retracts the probe to the top of the device. Impedances are re-created by moving the probe in the x and/or y directions using a tuner controller. The second coordinate controls the low band frequencies (4-11.9GHz) and the third, the high band frequencies (12-26.5GHz). Also, from experimental observations, it is assumed that the first coordinate controls the probe's movement in the x direction and the second and third, controls the movement in the y direction. Figure 3-3 shows the key moving components of a typical mechanical tuner.

3.4 Noise Measurement System Calibration

In order to measure any DUT, a number of critical steps are required before any measurements can take place. A full two port system calibration must be performed and system device characterization must also be determined for various source impedances. The system is calibrated using an on-wafer SOLT calibration substrate. After calibration, the thru line remains connected for system device characterization. A custom automated software system is design and

definitions can be found in Appendix B. Now, a complete s-parameter (S_{11} , S_{12} , S_{21} and S_{22}) measurement is taken to characterize the thru standard. Then changing connection of the switch from PNA port two to the NFA as shown in Figure 3-5. Then, by initiating a S_{11} measurement, Γ_{inr} is obtained by solving [21]

$$S_{11m} = S_{11} + \frac{S_{12}S_{21}\Gamma_{inr}}{1 - S_{22}\Gamma_{inr}} \quad (3.4)$$

where S_{11m} is the measured value and the s-parameters of the thru. This brings the reference plane to the input of the output probe. Therefore, the receiver block in Figure 3-4 consists of everything between the output probe and the NFA.

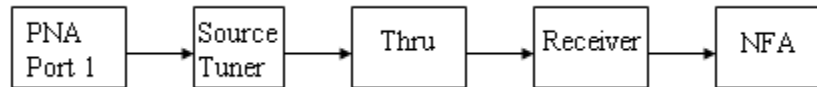


Figure 3-5: Output Impedance Path.

- Step 2) To obtain Γ_{ns} , the signal path as shown in Figure 3-6. The noise source is then replaced with an electronic calibration module (ECAL) and one port calibration of port two is executed, bringing the reference to output of the noise source. The noise source is place back and two S_{11} measurements (reflection coefficients) are taken for the hot and cold state (ie. noise source on/off).

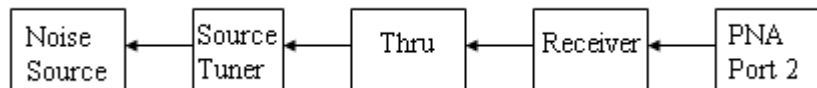


Figure 3-6: Source Tuner Characterization and Input Impedance Path.

- Step 3) The receiver which includes the load tuner, bias tee, switch, output wafer probe and the cables used to connect them is characterized by the port two error terms from full

two port calibration as discussed in this chapter and the complete error model is available in Appendix B.

- Step 4) To characterize the source tuner block which includes the source tuner, bias tee, switch, input wafer probe and the cables used to connect them, consider expression (3.5). From step 1-3, blocks thru, receiver and the sum of all the entire line (ie. Figure 3-6) are known based on the error term model in Appendix B.

$$\begin{aligned} \begin{bmatrix} S_{11} & S_{12} \\ S_{21} & S_{22} \end{bmatrix}_{SOURCE_TUNER} &= \begin{bmatrix} e'_{22} & 1 \\ e'_{23} & e'_{32} & e'_{33} \end{bmatrix}_{PNA_PORT_2_PATH} \begin{bmatrix} e'_{22} & 1 \\ e'_{23} & e'_{32} & e'_{33} \end{bmatrix}_{RECEIVER}^{-1} \begin{bmatrix} S_{11} & S_{12} \\ S_{21} & S_{22} \end{bmatrix}_{THRU}^{-1} \end{aligned} \quad (3.5)$$

To determine the source tuner, first the data is converted from s-domain data into *ABCD* domain data. The conversion details can be found in Appendix C. Once complete, using matrix computation to solve for the source tuner block and convert the data back from *ABCD* domain to S domain. The matrix equation used to solve for the source tuner is shown in (3.6).

$$\begin{bmatrix} A & B \\ C & D \end{bmatrix}_{SOURCE_TUNER} = \begin{bmatrix} A & B \\ C & D \end{bmatrix}_{PNA_PORT_2_PATH} \begin{bmatrix} A & B \\ C & D \end{bmatrix}_{RECEIVER}^{-1} \begin{bmatrix} A & B \\ C & D \end{bmatrix}_{THRU}^{-1} \quad (3.6)$$

This source tuner characterization is repeated at least four times at different source tuner positions (ie. source impedances) and the results will be used to solve for the noise parameters. In our case, the system used a list of 21 pre-determined source tuner positions that covered all four quadrants of the Smith chart. To achieve this, the noise source is replaced by the ECAL module and a port two calibration is commenced for a new source tuner position. This calibration characterizes the entire line as in Figure 3-6

and repeating the source tuner characterization step the new s-parameter information will be obtained at this tuner position.

- Step 5) Γ_s can be obtained using the expression given by [21]

$$\Gamma_s = S_{22} + \frac{S_{12}S_{21}\Gamma_{ns}}{1 - S_{11}\Gamma_{ns}}, \quad (3.7)$$

where the s-parameter used is obtained from the s-parameter matrix multiplication of the thru and source tuner and Γ_{ns} is from step 2.

- Step 6) Knowing the Γ information the impedance (Z) can be calculated using

$$Z = \frac{1}{Y} \quad (3.8)$$

where $Y = \frac{1 - \Gamma}{1 + \Gamma}$.

With all the S-parameter measurement data obtained, the next set of measurements will be to obtain the noise powers.

3.4.2 Noise Power Measurement and Noise Parameter Extraction

Switching to the noise path, hot and cold noise power measurements are taken using either a subset or all the source tuner positions from s-parameter measurement. With all the information obtained, using any of the extraction methods discussed, the noise parameters can be found. Our software system implemented the noise parameter extraction process developed by Chen *et al* and along with Lane's method for A , B , C and D extraction.

3.5 Software System Validation

The software system developed for this thesis is validated by comparing the source tuner characterization algorithm with an industry solution (ATS) developed by Maury Microwave. The

first set of results in Figures 3-7 to 3-14, shows the s-parameters of the source tuner for one source tuner position using the same calibration error terms.

Overall, the results are in good agreement of each other which confirms that both solutions are using similar source tuner characterization techniques. However, due to measurement and calibration uncertainties, certain data points are affected. The results show the magnitudes at certain points are the same with opposite signs. With respect to noise parameter extraction, only the absolute values are required so these differences will not affect the final results. It was concluded that the cause is likely due to instrument measurement uncertainty when reporting positive or negative results.

The next validation step is to confirm the *ABCD* extraction implementation. Figure 3-15 and 3-16, shows the measured and calculated noise powers in cold and hot states based on Lane's least squares fitting method. The experimental results are based on 15 different source impedances. The results show good agreement and further analysis showed that by using additional source impedance points the overall agreement in Figure 3-15 and 3-16 improve, but the calibration and measurement time increases for each additional point. This suggests that there exists a selection scheme that can achieve optimal results. Also, the noise power in the hot state experience slightly greater variation which is due to the uncertainty in effective source temperature. Therefore based on these results, the software solution implemented for this thesis is consistent with the current industry solution.

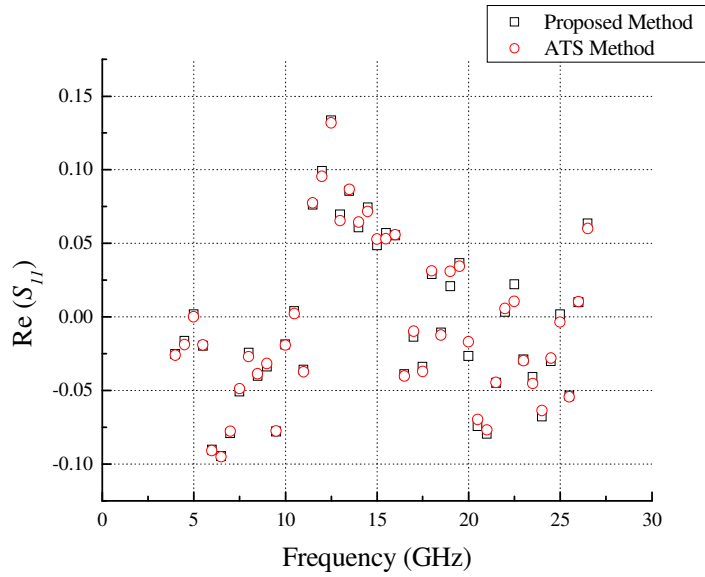


Figure 3-7: Real part of S_{11} , $\text{Re}(S_{11})$ using proposed and ATS method.

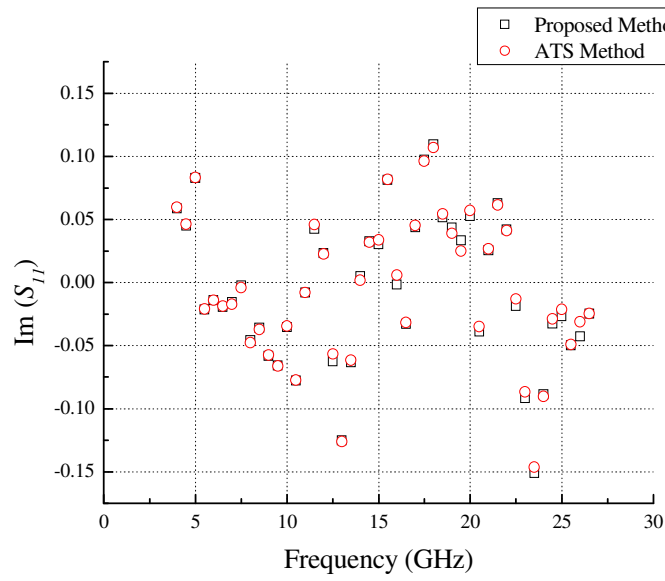


Figure 3-8: Imaginary part of S_{11} , $\text{Im}(S_{11})$ using proposed and ATS method.

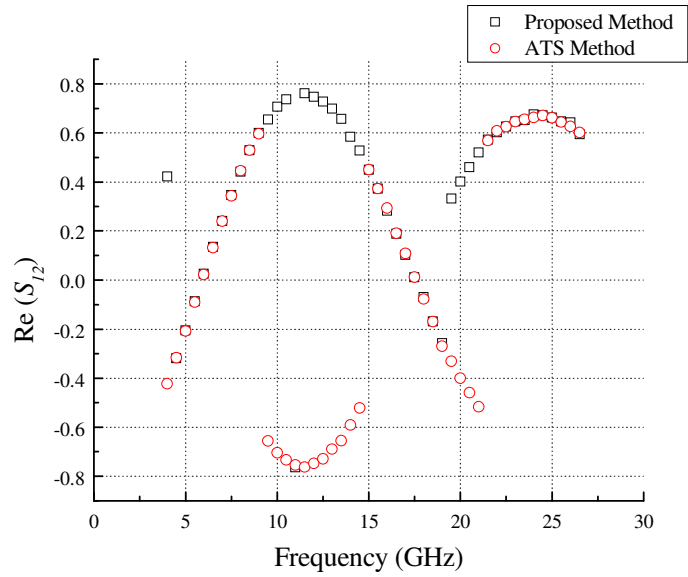


Figure 3-9: Real part of S_{12} , $\text{Re}(S_{12})$ using proposed and ATS method.

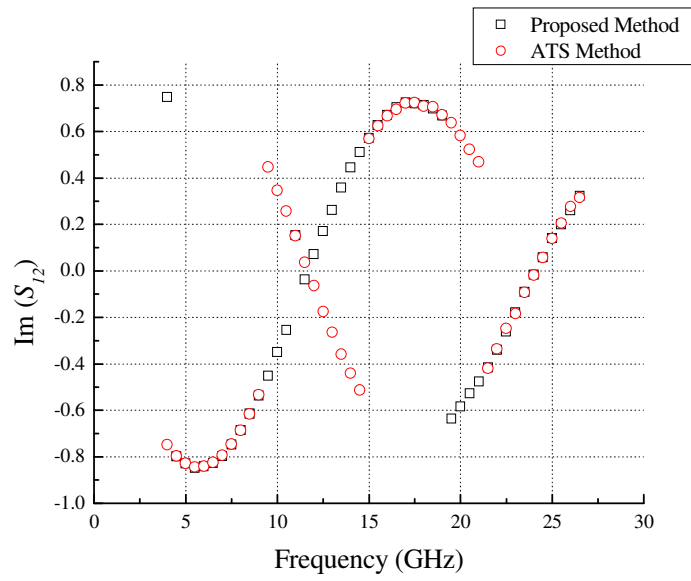


Figure 3-10: Imaginary part of S_{12} , $\text{Im}(S_{12})$ using proposed and ATS method.

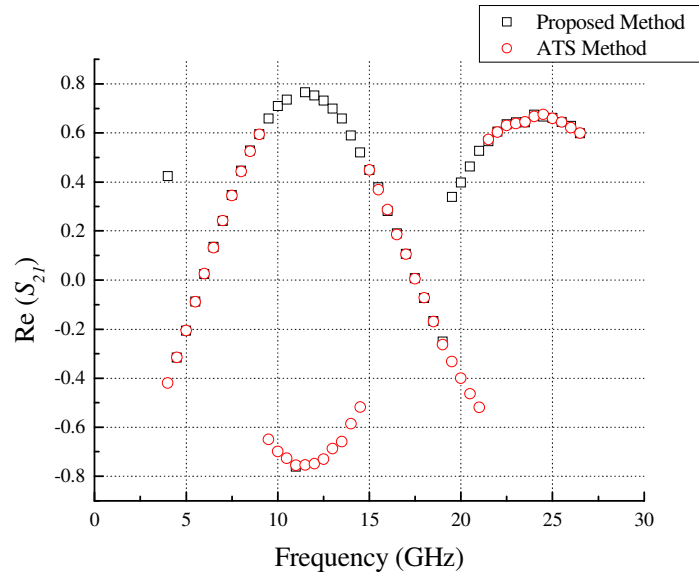


Figure 3-11: Real part of S_{21} , $\text{Re}(S_{21})$ using proposed and ATS method.

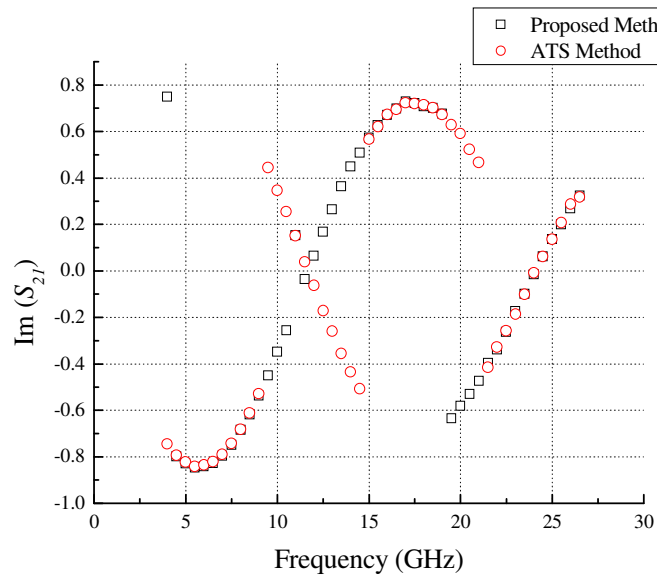


Figure 3-12: Imaginary part of S_{21} , $\text{Im}(S_{21})$ using proposed and ATS method.

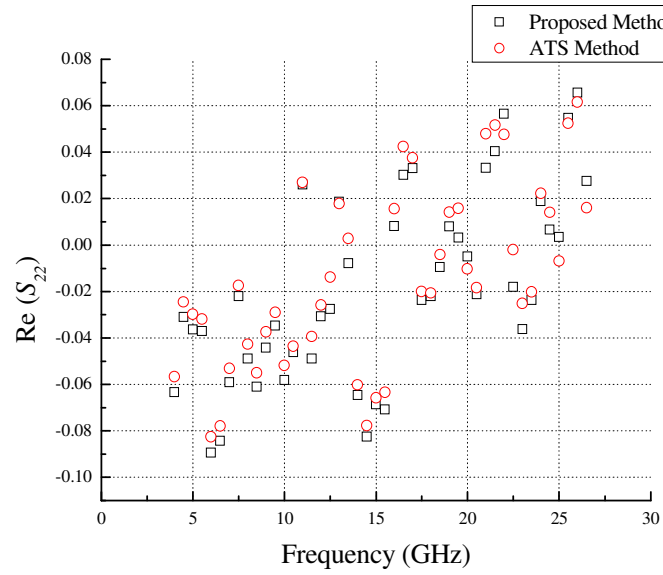


Figure 3-13: Real part of S_{22} , $\text{Re}(S_{22})$ using proposed and ATS method.

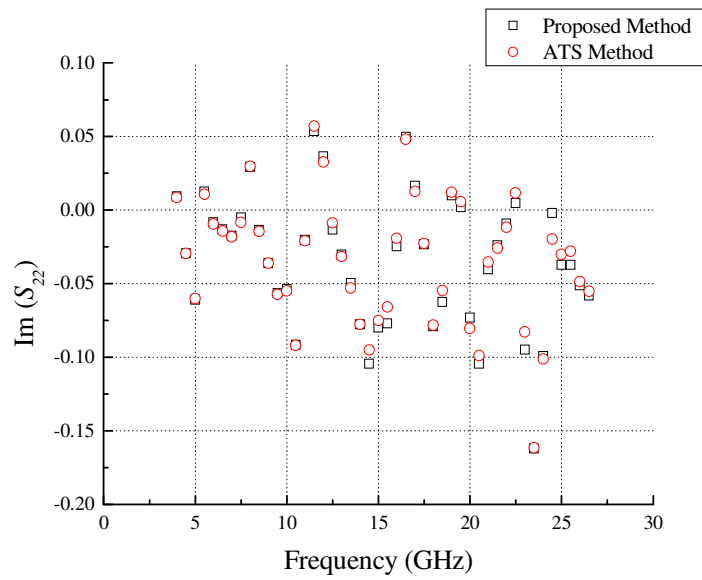


Figure 3-14: Imaginary part of S_{22} , $\text{Im}(S_{22})$ using proposed and ATS method.

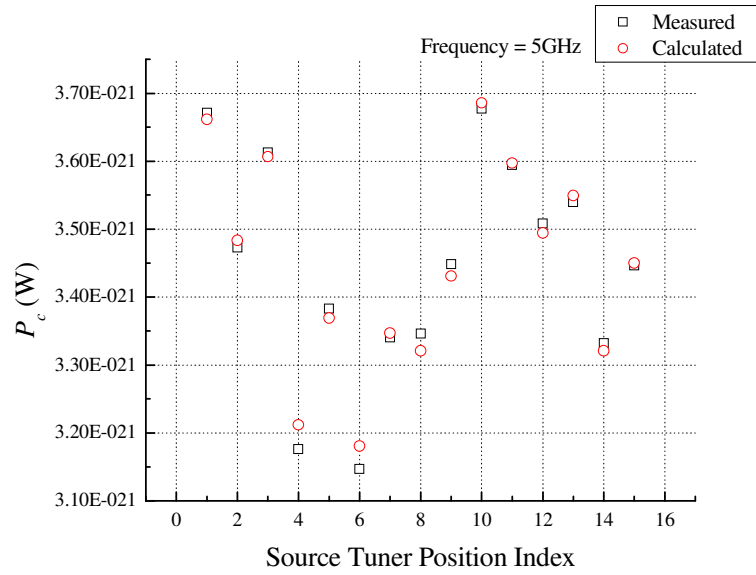


Figure 3-15: Noise power (P_c) measured vs. calculated (cold state) at 5GHz.

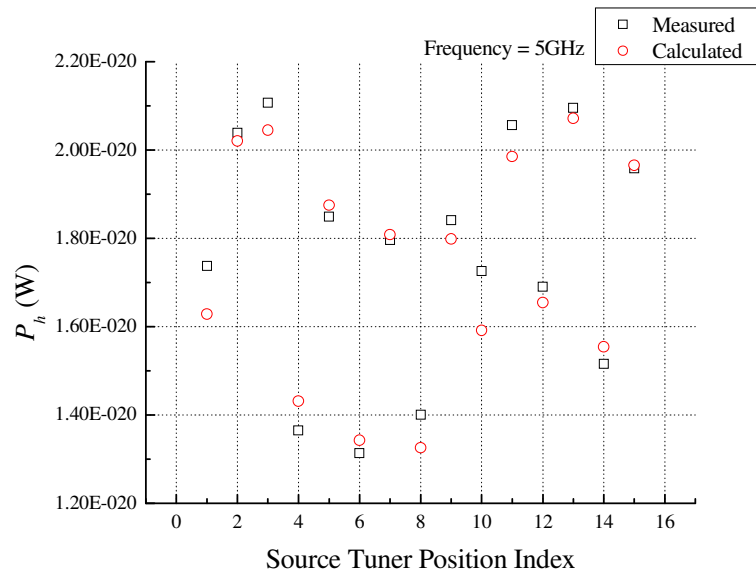


Figure 3-16: Noise power (P_h) measured vs. calculated (hot state) at 5GHz.

3.6 New Tuner Characterization Technique and Discussion

The new calibration procedure proposed in this thesis utilizes the ECAL module at the source tuner characterization stage as described in section 3.4.1, step 4. The current industry solution from Maury Microwave uses mathematical fitting techniques to estimate the s-parameters of the source tuner at different source impedances based on the default tuner position error terms obtained during system calibration. Our proposed solution takes advantage of the fast ECAL module which calibrates the system at the default tuner position and is repeated for all other tuner positions. Figure 3-17 to 3-24 shows the s-parameters of the tuner using the new calibration procedure at the default tuner position compared with the ATS method. Figure 3-25 to 3-32 shows the s-parameters of the tuner using the new characterization technique at position (2410, 265, 4500) and (905, 4500, 608) for low and high band frequencies respectively compared with the ATS method at the same tuner positions. The subtle differences the s-parameter data in the figures are due to the uncertainty in the calibration error term data used to characterize the source tuner. Also, during system validation it was shown that under the same conditions the source characterization of both software systems were in good agreement. As for the s-parameter data of the non-default position, observation shows that the data points begin to vary and differences is more noticeable in the S_{12} and S_{21} plots. This indicates uncertainty and error in the mathematical fitting approach used by the ATS system from Maury Microwave since our procedure continues to use actual calibration data instead of simulated data. Furthermore, our default position characterization method produced similar results. The new source tuner characterization approach for non-default positions relies on the ECAL module and follows the same algorithm used to characterize the source tuner at the default position. Therefore in conclusion, the new tuner characterization technique improves source tuner characterization and noise parameter accuracy in comparison to the current industry solution from Maury Microwave.

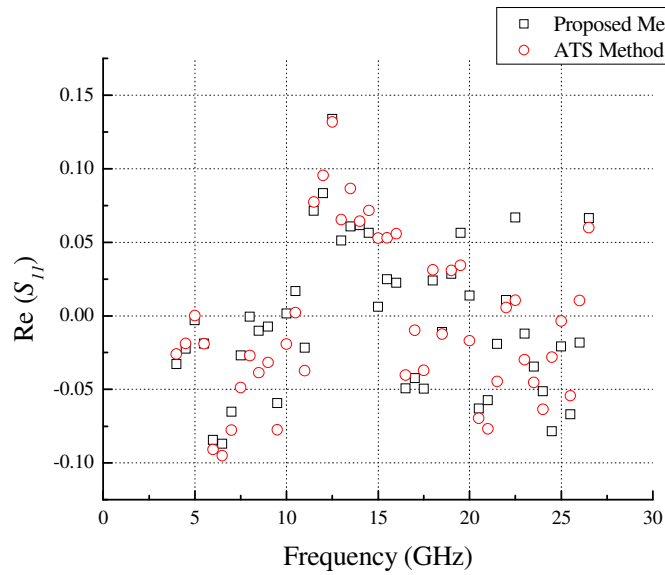


Figure 3-17: Real part of S_{11} , $\text{Re}(S_{11})$ using proposed and ATS method at position (100, 4500, 4500).

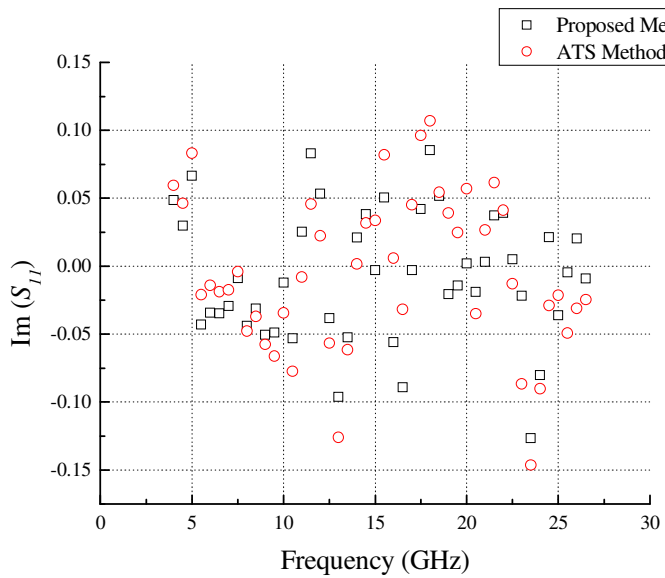


Figure 3-18: Imaginary part of S_{11} , $\text{Im}(S_{11})$ using proposed and ATS method at position (100, 4500, 4500).

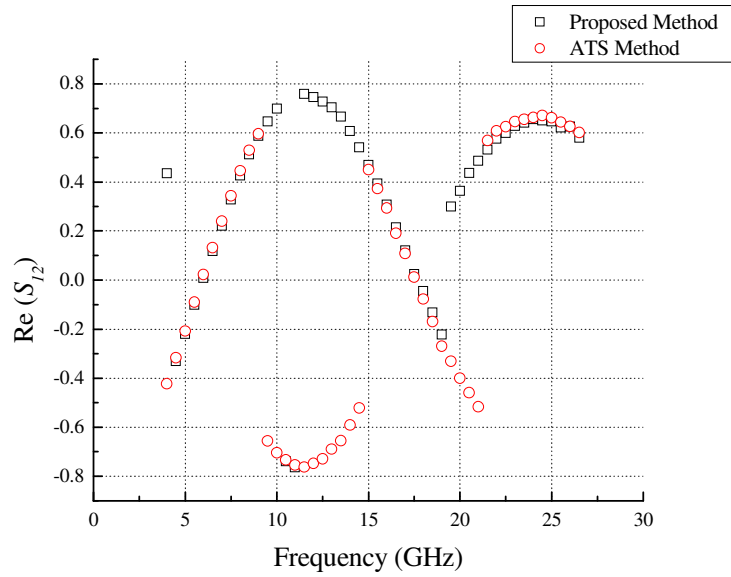


Figure 3-19: Real part of S_{12} , $\text{Re}(S_{12})$ using proposed and ATS method at position (100, 4500, 4500).

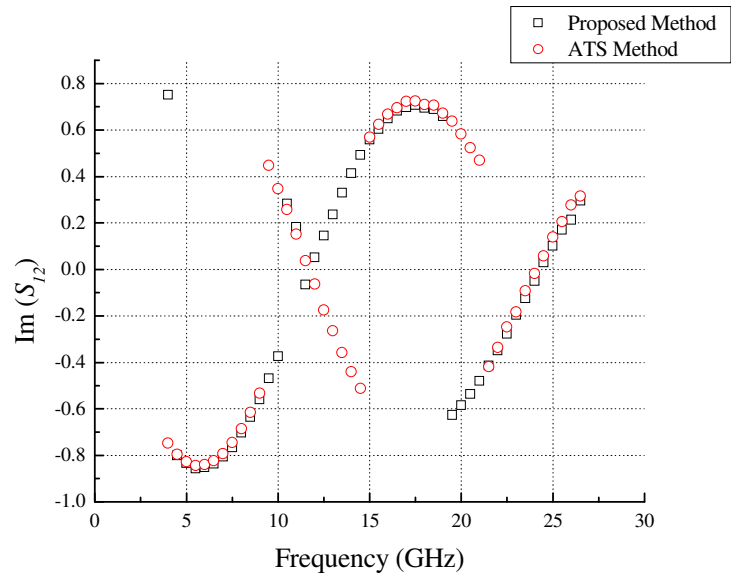


Figure 3-20: Imaginary part of S_{12} , $\text{Im}(S_{12})$ using proposed and ATS method at position (100, 4500, 4500).

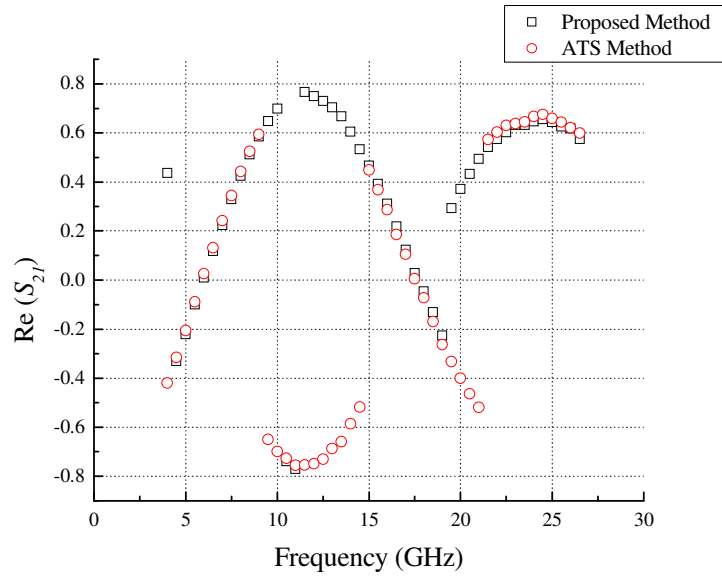


Figure 3-21: Real part of S_{21} , $\text{Re}(S_{21})$ using proposed and ATS method at position (100, 4500, 4500).

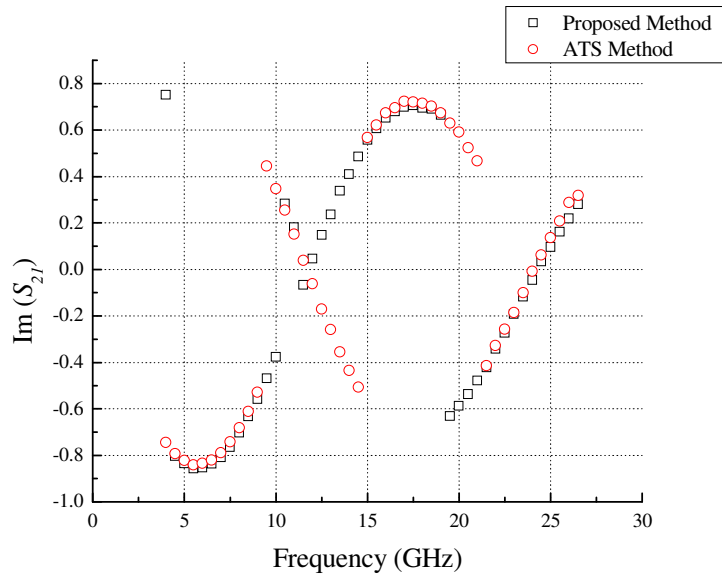


Figure 3-22: Imaginary part of S_{21} , $\text{Im}(S_{21})$ using proposed and ATS method at position (100, 4500, 4500).

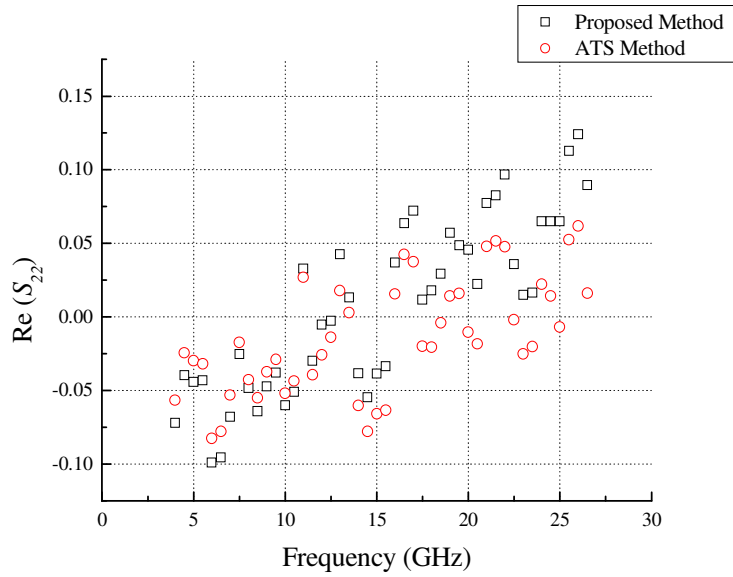


Figure 3-23: Real part of S_{22} , $\text{Re}(S_{22})$ using proposed and ATS method at position (100, 4500, 4500).

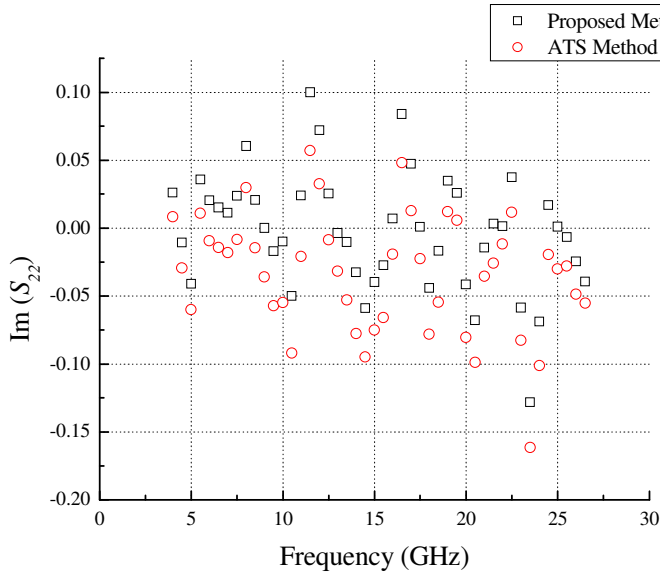


Figure 3-24: Imaginary part of S_{22} , $\text{Im}(S_{22})$ using proposed and ATS method at position (100, 4500, 4500).

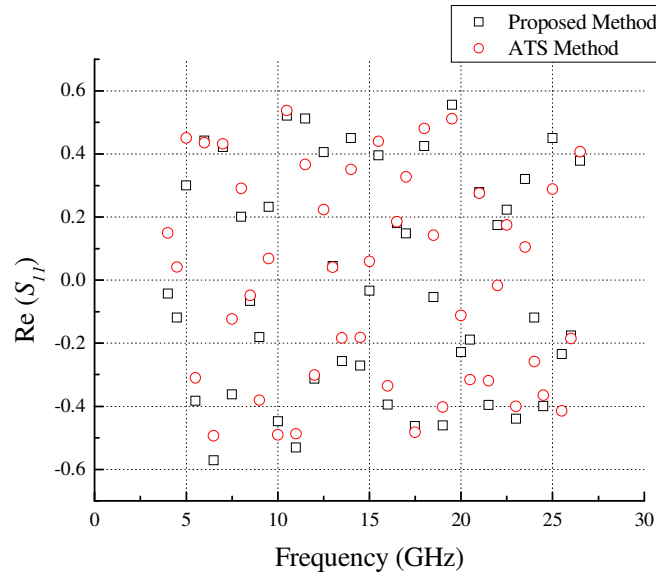


Figure 3-25: Real part of S_{11} , $\text{Re}(S_{11})$ using proposed and ATS method at (2410, 632, 4500) and (908, 4500, 608) positions for low and high band respectively.

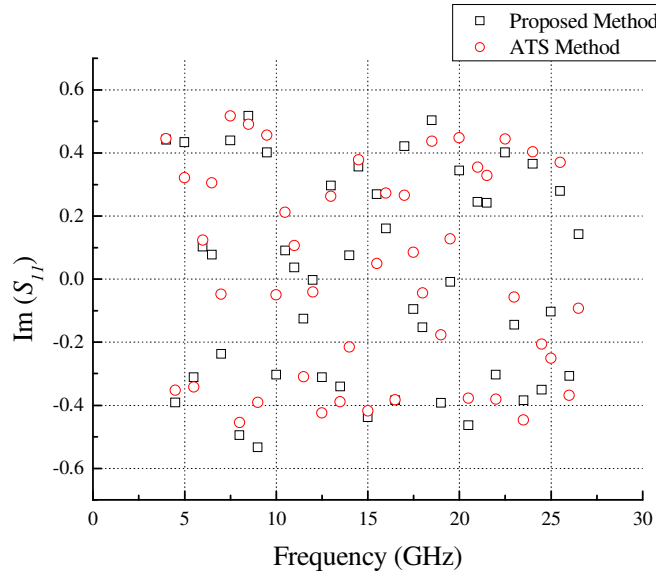


Figure 3-26: Imaginary part of S_{11} , $\text{Im}(S_{11})$ using proposed and ATS method at (2410, 632, 4500) and (908, 4500, 608) positions for low and high band respectively.

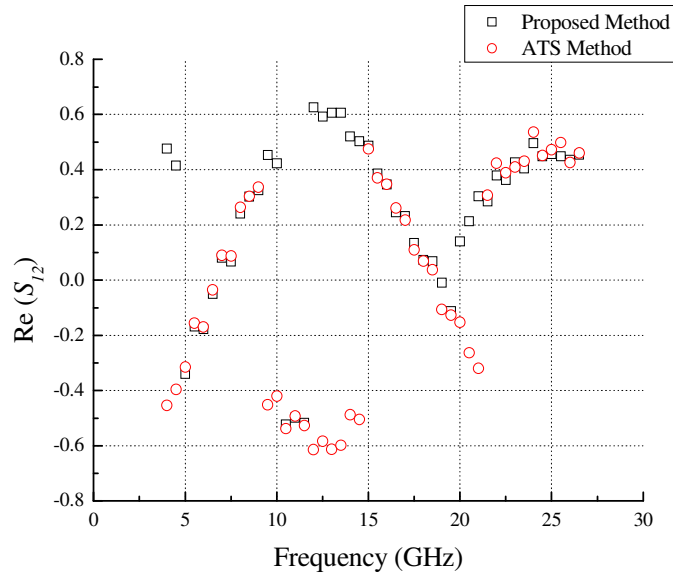


Figure 3-27: Real part of S_{12} , $\text{Re}(S_{12})$ using proposed and ATS method at (2410, 632, 4500) and (908, 4500, 608) positions for low and high band respectively.

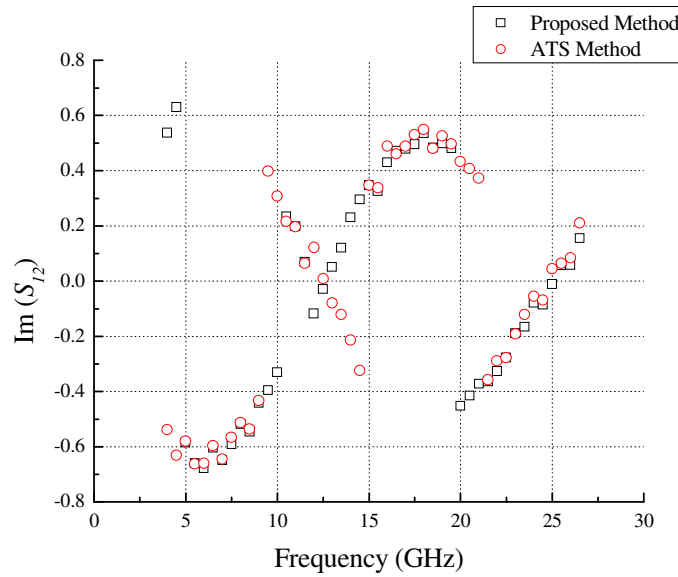


Figure 3-28: Imaginary part of S_{12} , $\text{Im}(S_{12})$ using proposed and ATS method at (2410, 632, 4500) and (908, 4500, 608) positions for low and high band respectively.

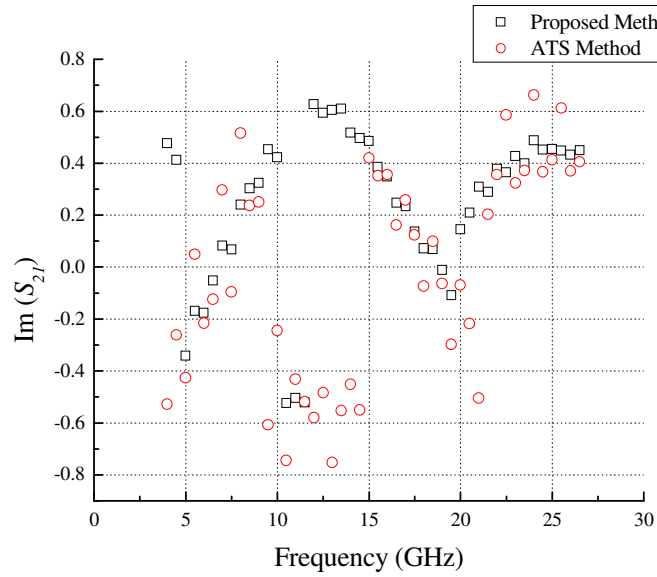


Figure 3-29: Real part of S_{21} , $\text{Re}(S_{21})$ using proposed and ATS method at (2410, 632, 4500) and (908, 4500, 608) positions for low and high band respectively.

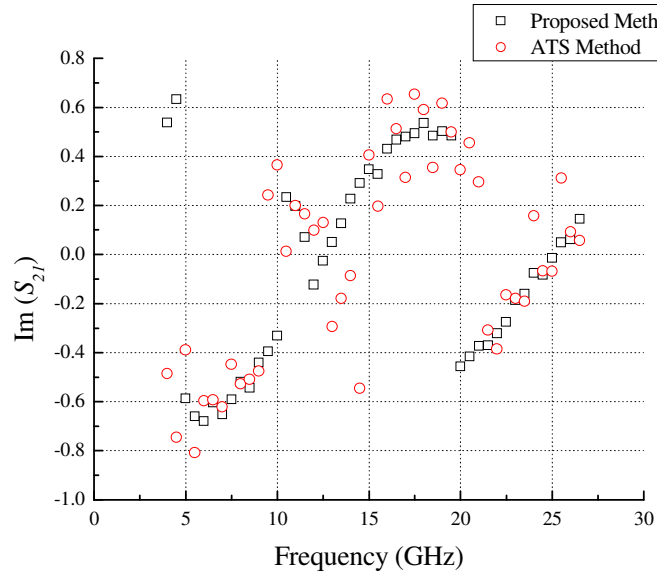


Figure 3-30: Imaginary part of S_{21} , $\text{Im}(S_{21})$ using proposed and ATS method at (2410, 632, 4500) and (908, 4500, 608) positions for low and high band respectively.

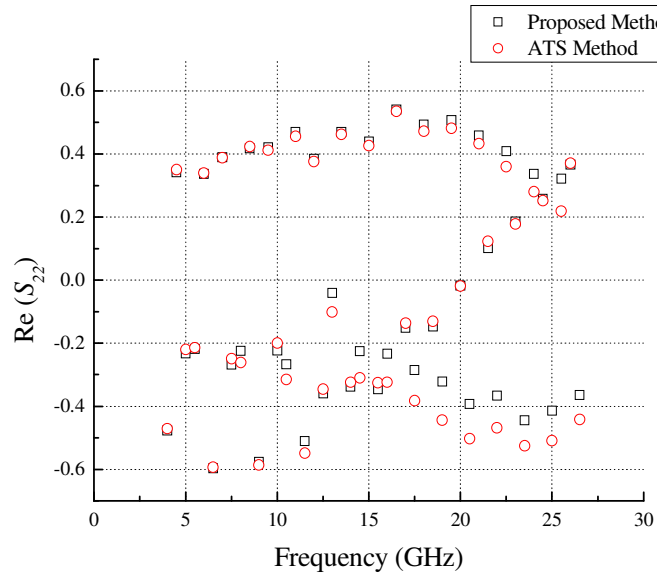


Figure 3-31: Real part of S_{22} , $\text{Re}(S_{22})$ using proposed and ATS method at (2410, 632, 4500) and (908, 4500, 608) positions for low and high band respectively.

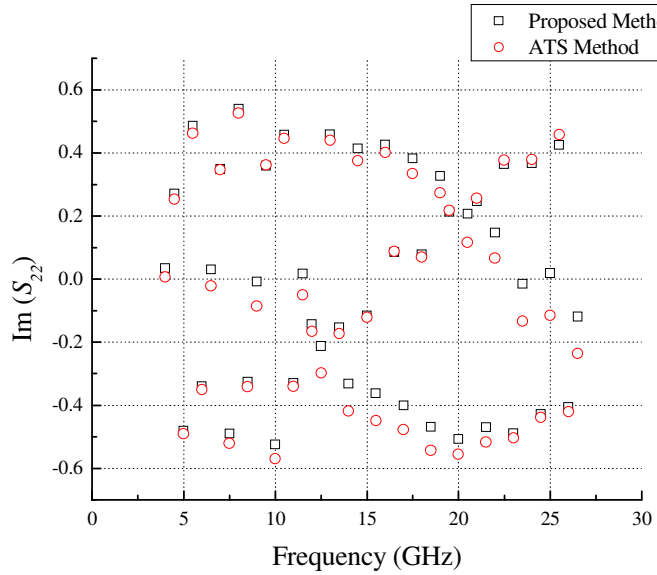


Figure 3-32: Imaginary part of S_{22} , $\text{Im}(S_{22})$ using proposed and ATS method at (2410, 632, 4500) and (908, 4500, 608) positions for low and high band respectively.

Chapter 4

New Gain Compensation Technique

Noise power measurement is a critical step in noise parameter extraction and any uncertainties will directly impact device characterization results. The new gain compensation technique proposes a systematic procedure to correct all measured noise powers used in noise parameter extraction. This chapter discusses the receiver gain experimental results observed and proposes the new gain compensation technique and its experimental results.

4.1 Receiver Gain Analysis

Figure 4-1 and 4-2 shows the receiver gain (G_0) with respect to source impedance for 5 and 25GHz respectively. It appears that the error fluctuation in the gain is a function of source impedance and increases with it. According to the figures, it can be seen that the error causes data points to shift away from approximately 0.3 at 5GHz and 0.019 at 25GHz as $|\Gamma_s|$ increases. The figures also demonstrate that source tuner positions that represent smaller $|\Gamma_s|$ should be chosen for noise parameter extraction as the impacts from error is minimized. In other words choosing source tuner positions that lie closer to the centre of the Smith chart will result in improved noise parameter accuracy.

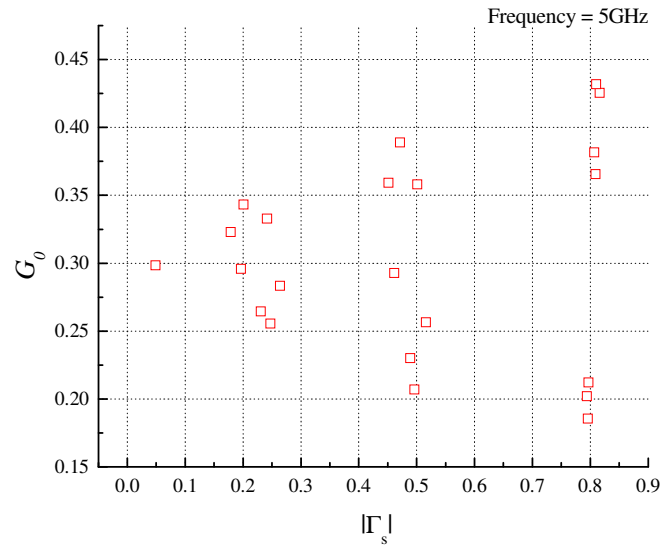


Figure 4-1: Measured Receiver Gain, G_0 (linear value) versus Γ_s at 5GHz.

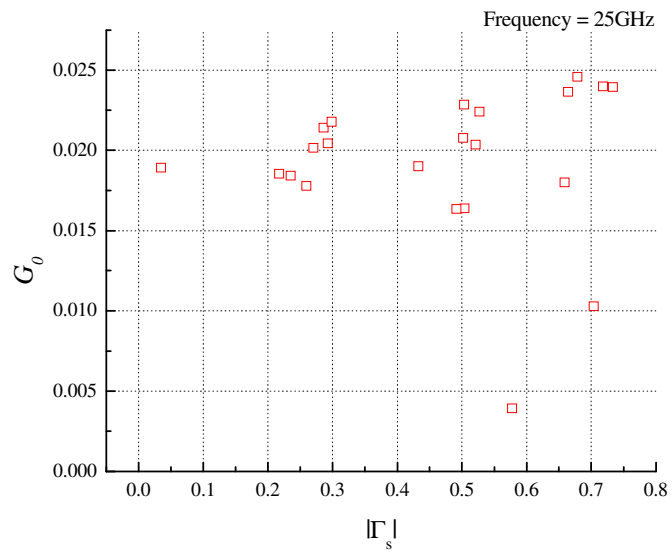


Figure 4-2: Measured Receiver Gain, G_0 (linear value) versus Γ_s at 25GHz.

4.2 New Gain Compensation Technique

Based on Chen *et al.*'s method the least-squares fit approach is applied to the expression given by [14]

$$\frac{P_n G_s}{kT_0 \Delta f} \cdot \frac{|1 - \Gamma_{inr} \Gamma_s|^2}{1 - |\Gamma_s|^2} = (T_{seffnor} G_s + |Y_s|^2 A + B + 2G_s C + 2B_s D) G_0. \quad (4.1)$$

By re-arranging this expression, it becomes

$$|Y_s|^2 \times A + B + 2G_s \times C + 2B_s \times D = G_s \left(\frac{P_n}{kT_0 \Delta f G_0} \cdot \frac{|1 - \Gamma_{inr} \Gamma_s|^2}{1 - |\Gamma_s|^2} - T_{seffnor} \right). \quad (4.2)$$

Given that the noise parameters are a function of A , B , C and D , the error from the measured noise power will ultimately affect the noise parameter extraction accuracy. To determine the proposed gain compensation correction factor, the following steps are performed:

- Step 1) Calibrate system with a frequency range equal to the IF bandwidth setting of the NFA (i.e., 4MHz) with the center frequency equal to the desired frequency for measurement.
- Step 2) Calculate the available power gain of the source impedance tuner (G_{avt}) which is given by (4.3) for all source impedances used during system calibration.

$$G_{avt} = \frac{(1 - |\Gamma_{ns}|^2) |s_{21}|^2}{|1 - s_{11} \Gamma_{ns}|^2 \left(1 - \left| s_{22} + \frac{s_{12} s_{21} \Gamma_{ns}}{1 - s_{11} \Gamma_{ns}} \right|^2 \right)}, \quad (4.3)$$

- Step 3) Determine the percent variation of G_{avt} which is given by (4.4) for all source impedances normalized to the center frequency (desired frequency).

$$Percentage_Variation = \frac{\sum G_{avt} - G_{avt_cf}}{N_{pt} G_{avt_cf}} \times 100\%, \quad (4.4)$$

where

N_{pt} is the total number of source impedances,

G_{avt_cf} is the power gain at the desired frequency and

$\sum G_{avt}$ is the sum of power gains for all sources impedances.

- Step 4) Percent variations are applied to all the corresponding measured noise powers. Then with the corrected data, new A , B , C and D and noise parameters results can be obtained.

4.2.1 Experimental Results

Figure 4-3 and 4-4 shows the G_{avt} variation at 5GHz and 25GHz respectively for one source impedance. The figures show results at our desired frequencies over a span of 4MHz, which is the IF bandwidth setting of the NFA. At this tuner position (Maury Microwave default tuner position), the minimum and maximum values are 0.7446 and 0.7457 at 5GHz and 0.462 and 0.472 at 25GHz respectively. When making noise measurements, it is assumed that the DUT has an amplitude versus frequency characteristics that is constant over the IF bandwidth (4MHz in our case) [4]. Clearly the system gain is not constant within this range and with these gain fluctuations, uncertainties at the noise power measurement stage are likely. Typically, the NFA reports the mean noise level within the bandwidth in order to minimize the impact of jitter noise (a random noise), so it is important to use a wide bandwidth and have constant system characteristics for better noise measurement [4]. Also, it can be seen that the gain fluctuation increase moving into higher frequencies for the same source impedance and the overall gain decreases due to an increase in system leakage at higher frequencies.

Figure 4-5 and 4-6 shows the calculated percentage variation at 5GHz and 25GHz respectively for all calibrated source impedances used in this test case. At 5GHz, the largest variation is 1.6% but generally, most source impedances are less than $\pm 0.5\%$. This demonstrates that at lower frequencies, noise measurement error is relatively low. However, at 25GHz, the variation is as high as -27% which means the measured value is undervalued by this amount. Overall, at high frequencies, greater variations are seen at more source impedances than what is seen at lower frequencies. These higher variations can be attributed to the larger fluctuation levels experienced as seen in Figure 4-4. These results first demonstrate that there is a direct relationship with the percent variation calculated and frequency. This observation is consistent in that at higher frequencies there is more system leakage and experimental uncertainty [14]. Secondly, it also shows that source impedance selection can affect noise parameter extraction accuracy. Figure 4-5 and 4-6 give an indication on which source impedances are good and which too avoid. These observations are inline with previous studies [14].

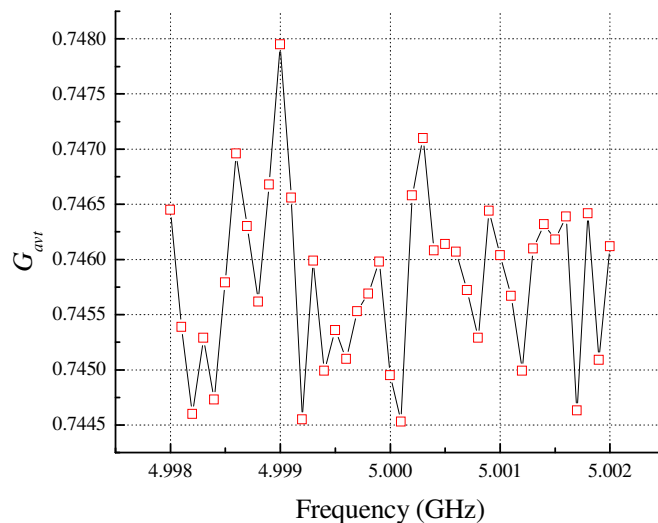


Figure 4-3: Measured Available Power Gain, G_{avt} (linear value) variation for one source impedance at 5GHz.

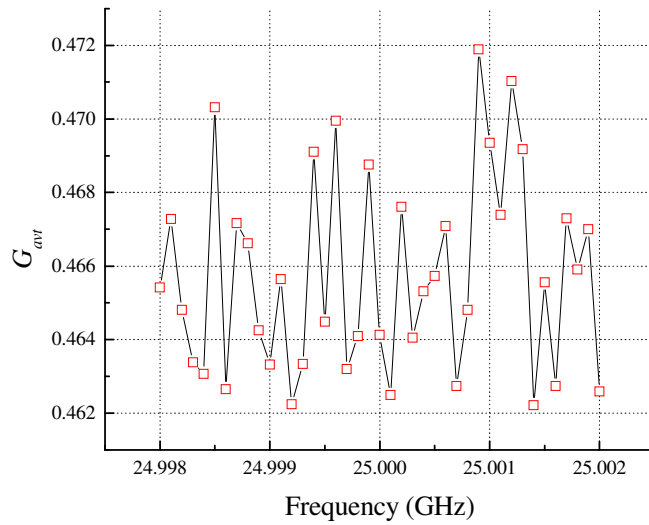


Figure 4-4: Measured Available Power Gain, G_{avt} (linear value) variation for one source impedance at 25GHz.

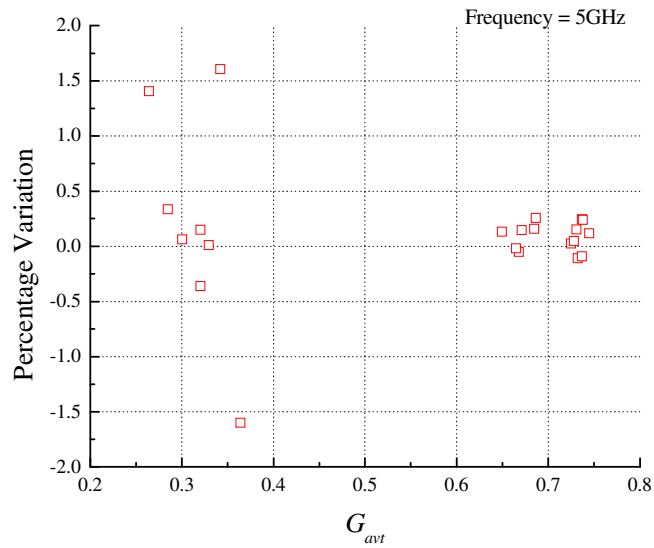


Figure 4-5: Calculated percentage variation for different source impedances at 5GHz.

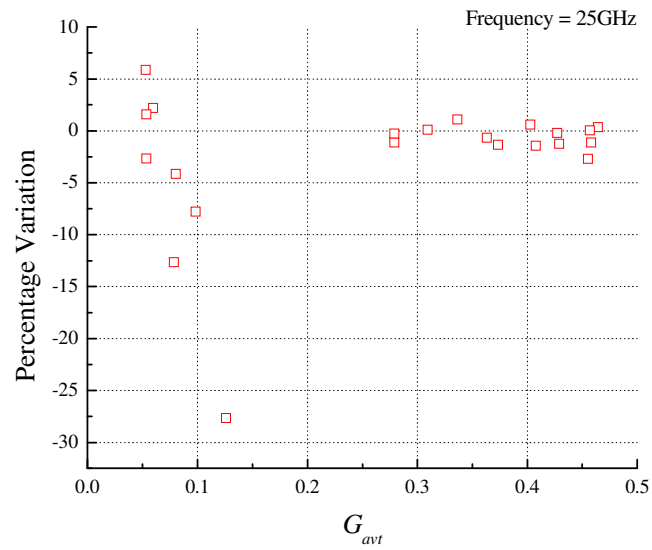


Figure 4-6: Calculated percentage variation for different source impedances at 25GHz.

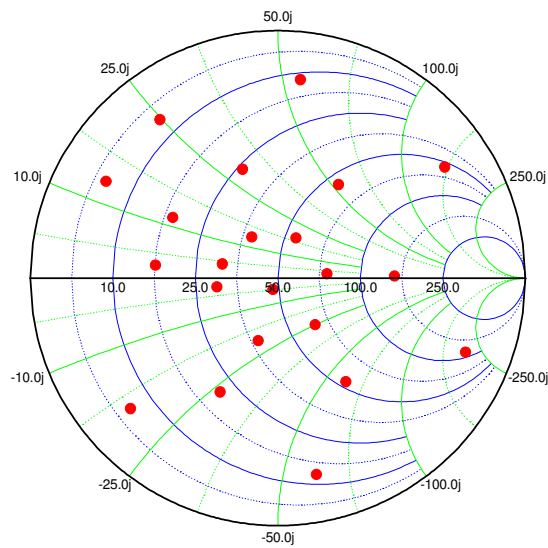


Figure 4-7: Source Impedance Smith Chart Coverage at 5GHz.

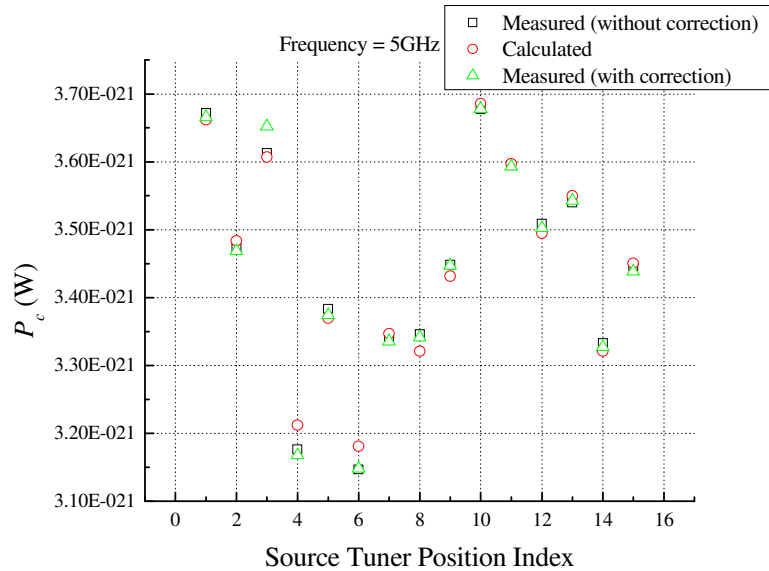


Figure 4-8: Comparison of Noise Power (P_c) measured with and without correction and calculated at 5GHz.

Figure 4-1 and 4-2 reinforces the importance of source impedance selection for noise parameter extraction since at high Γ positions, there is large gain fluctuation. This information provides a simple method to identifying undesirable tuner positions for noise parameter extraction. This result also contradicts Adamian and Uhlir method's assumption of a constant K for all source impedances. Figure 4-7 shows the original 21 source impedance selection for this thesis provides good Smith chart coverage. Figure 4-8 shows the comparison between the uncorrected, calculated and corrected noise powers. It was determined that 7 of the pre-determined source impedances should not be used for fitting. Therefore, the $ABCD$ values used to calculate the simulated noise powers are based on the best 14 source impedances. From this comparison, it is clearly seen that certain data points move closer to the calculated (or simulated) value while others move away relative to the uncorrected data point. To measure the overall

effectiveness of the proposed method a new Figure of Merit (*FOM*) is required. The *FOM* developed to evaluate the proposed gain compensation technique is expressed by

$$FOM = \frac{\sum_{i=1}^N \left| \frac{P_c - P_{c_sim}}{P_c} \right|}{N} \quad (4.6)$$

where P_c is the uncorrected or corrected measured noise power, P_{c_sim} is the corresponding simulated noise power and N is the total number of data points.

This *FOM* compares the total error seen from the measured noise powers (uncorrected or corrected) and the simulated noise power determined from the extracted *ABCD* data. Table 4-1 shows the calculated results of the *FOM*. Based on this data, the proposed gain compensation technique does not lower the total error. In fact, by only using the optimal source tuner positions, the noise power uncertainty is almost negligible. However, this thesis still confirms that measurement uncertainty is present in the measured noise power and further improvements to noise parameter accuracy can still be achieved. Table 4-2 shows the noise parameters and gain of the receiver from 5 to 25GHz, with a 2GHz frequency step using 14 source impedances for *ABCD* determination. All high Γ positions were removed for improved noise parameter extraction accuracy. In conclusion, the experimental results demonstrate that source impedance selection is a major source of measurement uncertainty and possibly the most dominant factor impacting noise parameter accuracy.

Table 4-1: Figure of Merit for Noise Power Correction Method.

Freq (GHz)	FOM (Uncorrected)	FOM (Corrected)
5	0.00410	0.00494
7	0.01100	0.0116
9	0.01100	0.01298
11	0.00580	0.00875
13	0.00427	0.0041
15	0.00446	0.0097
17	0.00703	0.0092
19	0.00534	0.0195
21	0.00489	0.0125
23	0.00334	0.0061
25	0.00826	0.0102

Table 4-2: Extracted Noise Parameters and Gain G_0 of the Receiver in the Calibration Stage for Corrected and Uncorrected (values in brackets) Noise Powers.

Freq (GHz)	$N_{F_{min}}$ (dB)	R_n (Ω)	$ \Gamma_{opt} $	$\angle \Gamma_{opt}$ ($^\circ$)	G_0 (dB)
5	3.61	7.65	0.50	-175	-5.24
	(3.61)	(8.06)	(0.49)	(-175)	(-5.24)
7	3.78	8.61	0.51	-167	-6.71
	(3.84)	(9.22)	(0.50)	(-167)	(-6.71)
9	3.93	13.49	0.49	-151	-8.47
	(3.94)	(13.37)	(0.49)	(-152)	(-8.47)
11	4.35	20.55	0.30	-147	-10.15
	(4.36)	(20.27)	(0.31)	(-146)	(-10.16)
13	3.81	17.56	0.29	-146	-10.46
	(3.80)	(17.48)	(0.29)	(-145)	(-10.45)
15	4.20	16.59	0.32	-168	-11.56
	(4.21)	(16.20)	(0.32)	(-169)	(-11.56)
17	3.78	16.93	0.35	-140	-11.39
	(3.75)	(17.38)	(0.35)	(-140)	(-11.40)
19	4.59	16.26	0.38	-158	-12.83
	(4.63)	(17.07)	(0.37)	(-159)	(-12.82)
21	5.30	24.75	0.27	-154	-14.55
	(5.30)	(26.22)	(0.25)	(-157)	(-14.54)
23	6.37	43.46	0.23	-126	-16.51
	(6.35)	(43.09)	(0.22)	(-129)	(-16.53)
25	6.98	50.65	0.11	-147	-17.19
	(6.94)	(54.28)	(0.10)	(-141)	(-17.20)

Chapter 5

Conclusion

Noise theory and measurement have been thoroughly reviewed in this thesis. The subjects reviewed include: electronic noise, instrument calibration theory and measurement uncertainty and noise parameter extraction methods. This thesis presented a newly automated software system that was designed and verified for on-wafer noise measurement, a new tuner characterization technique that improves source tuner characterization is discussed and a new gain compensation technique that attempts to improve noise parameter extraction is proposed. The results of this method showed that the available power gain of the source tuner does not remain constant within a 4MHz bandwidth which causes measurement uncertainty at the noise power measurement stage. However, this proposed new method did not improve the accuracy of noise parameter, but demonstrated that a correction to the measured noise power measurement is valid and required. Furthermore, our results demonstrate that source tuner positions that lie closest to the centre of the Smith chart will produce the most optimal and accurate results. Also, there exists a need to determine an optimal number of impedance points to use for noise parameter extraction that will yield the highest overall performance between calibration time and accuracy.

5.1 Future Software Upgrades

The software system is scalable and can be upgraded to include additional functionality. The system currently is designed primarily for on-wafer noise measurement. Other functions have been explored and the development of the following capabilities has commenced.

- Decision Maker is designed solely for source impedance selection. Noise parameter extraction methods are highly sensitive to this selection as described and shown in this thesis.
- S11 Cal is designed to calibrate the line beginning from PNA port 1 to the switch, which brings the noise reference plane to the input of the LNA.
- S11 Measurement is designed to take a S_{11} measurement to obtain the Γ_{in} . This is to be used in conjunction with S11 Cal.
- NFA Cal is an automated procedure that executes the calibration of the NFA.

5.2 Possible Future Research Areas

The results of this thesis provided insight on new research areas that can further improve noise parameter extraction accuracy. The results of this thesis showed a need to correct the measured noise power directly and that there is potential improvements to extraction accuracy. Additional research can lead to an improved compensation technique. The least-squares fit approach theoretically only requires four independent sets of measurement data. However, accuracy is highly dependent on two factors: source impedance selection in general as well as custom selection for each desired frequency and total number of data sets used for fitting. Further research in these areas will prove to be valuable information in improving noise parameter accuracy.

References

- [1] A. van der Ziel, *Noise in Solid State Devices and Circuits*, New York, John Wiley & Sons, Inc., 1986.
- [2] F. N. Hooge, “ $1/f$ Noise”, *Physica*, vol. 83B, p. 14, 1976.
- [3] H. T. Friis, “Noise figures of radio receivers,” *Proc. IRE*, vol. 32, no. 7, pp. 419–422, Jul. 1944.
- [4] *Agilent Fundamentals of RF and Microwave Noise Figure Measurements*, pp. 1-31. Agilent Application Note 57-1.
- [5] A. Fantom, *Radio Frequency & Microwave Power Measurements*, London, U.K.: Peter Peregrinus Ltd, 1990.
- [6] IRE Subcommittee on Noise, 59 IRE 20. S1, “IRS standards on methods of measuring noise in linear twoports, 1959,” *Proc. of the IRE*, vol. 48, no. 1, pp. 60-68, Jan. 1960.
- [7] R. Q. Lane, “The determination of device noise parameters,” *Proc. of the IEEE*, vol. 57, no. 8, pp. 1461-1462, Aug. 1969.
- [8] V. Adamian and A. Uhlir, “A novel procedure for receiver noise characterization,” *IEEE Trans. Instrumentation and Measurement*, vol. IM-22, no. 2, pp. 181-182, June 1973.
- [9] G. Caruso and M. Sannino, “Computer-aided determination of microwave two-port noise parameters,” *IEEE Trans. Microwave Theory Tech*, vol. MTT-26, no. 9, pp. 639-642, 1978.
- [10] J. Lange, “Noise characterization of linear twoports in terms of invariant parameters,” *IEEE J. Solid-State Circuits*, vol. SC-2, no. 2, pp. 37-40, June 1967.
- [11] J. M. O’Callaghan and J. P. Mondal, “A vector approach for noise parameter fitting and selection of source admittances,” *IEEE Trans. Microwave Theory Tech*, vol. 39, no. 8, pp. 1376-1382, Aug. 1991.
- [12] M. Mitama and H. Katoh, “An improved computational method for noise parameter measurement,” *IEEE Trans. Microwave Theory and Tech.*, vol. MTT-27, no. 6, pp. 612-615, 1979.
- [13] A. C. Davidson, B.W. Leake and E. Strid, “Accuracy improvements in microwave noise parameter measurements,” *IEEE Trans. Microwave Theory Tech*, vol. 37, no. 12, pp. 1973-1978, Dec. 1989.
- [14] Chih-Hung Chen, Ying-Lien Wang, Mohamed H. Bakr, Zheng Zeng “Novel Noise Parameter Determination for On-Wafer Microwave Noise Measurements” *IEEE Transactions on Instrumentation and Measurement*, vol 57, no. 11, November 2008
- [15] Agilent Technologies, Inc. “*Agilent Network Analyzer Basics*”, Printed in USA, August 31, 2004
- [16] Rytting, Doug, “*Network Analyzer Error Models and Calibration Methods*” Agilent Technologies, Inc.
- [17] Dr. B. Frank, “*Network Parameters*”, Queen’s University, 2007
- [18] *Noise Figure Measurement Accuracy – The Y-factor Method*, pp. 1-45. Agilent Application Note 57-2.
- [19] Chih-Hung Chen, “Accuracy Issues of On-Wafer Microwave Noise Measurements,” McMaster University, May 2008.
- [20] Hiebel, Micheal, “Vector Network Analyzer (VNA) Calibration: The Basics,” Rohde & Schwarz 2008.
- [21] *10 Hints for Making Successful Noise Figure Measurements*, Agilent Application Note 57-3.

- [22] Andries J. Scholten *et al.*, “Noise Modeling for RF CMOS Circuit Simulation,” *IEEE Trans. Electron Devices*, vol. 50, no.3, pp. 618-632, 2003.
- [23] *S-Parameter Design*, Agilent Application Note 154.
- [24] Agilent Technologies, Inc. “Agilent Specifying Calibration Standards for the Agilent 8510 Network Analyzer”, Printed in USA, July 13 2006
- [25] Agilent Technologies, Inc. “Specifying Calibration Standards and Kits for Agilent Vector Network Analyzers”, Printed in USA, April 14 2010
- [26] *Understanding Directivity*, Anritsu Application Note, USA, March 2008
- [27] Theory of Noise Measurements, Jul. 6, 1999, Maury Microwave. Application Note: 5C-042.
- [28] M.W. Medley, *Microwave and RF Circuits: Analysis, Synthesis and Design*. Norwood, MA: Artech House, 1993.
- [29] *International Technology Roadmap for Semiconductors (ITRS)*, 2005.
- [30] R. Meierer and C. Tsironis, “An on-wafer noise parameter measurement technique with automatic receiver calibration,” *Microw. J.*, vol. 38, no. 3, pp.22-27, Mar. 1995.
- [31] P. R. Gray, “Analysis and design of analog integrated circuits,” Fourth edition, John Wiley & Sons Inc., 2001.
- [32] M. L. Schmatz and H. R. Benedickter, “Accuracy Improvements in Microwave Noise Parameter Determination,” 51st ARFTG Conference Digest, pp. 62-64, 1998.
- [33] C. H. Chen, M. Jamal Deen, Yuhua Cheng and Mishel Matloubian, “Extraction of the induced gate noise, channel noise and their correlation in submicron MOSFETs from RF noise measurements,” *IEEE Trans. Electron Devices*, vol. 38, no. 12, pp. 2884-2892, 2001.
- [34] M. W. Pospieszalski, “On the measurement of noise parameters of microwave two-port,” *IEEE Trans. Microwave Theory Tech*, vol. 34 no. 4, pp. 456-458, 1986.
- [35] *Agilent Noise Figure Analyzer NFA Series Calibration and Performance Verification Guide*, Agilent Technology, Santa Clara, CA, 2001.
- [36] *On-Wafer Vector Network Analyzer Calibration and Measurements*, Cascade Microtech Application Note.
- [37] H. Rothe and W. Dahlke, “Theory of noisy fourpoles,” *Proceedings of the IRE*, pp. 811-818, June 1956.
- [38] 2. IRE Standards Committee, “IRE standards on methods of measuring noise in linear twoports, 1959,” *Proceedings of the IRE*, pp. 60-68, January 1960.
- [39] K. Hartmann, W. Kotyczka and M. Strutt, “Computerized determination of electrical network noise due to correlated and uncorrelated noise sources,” *IEEE Trans. Circuit Theory*, pp. 321-322, May 1973.
- [40] H. Hillbrand and P. Russer, “An efficient method for computer aided noise analysis of linear amplifier networks,” *IEEE Trans. Circuits and Systems*, vol. CAS-23, no. 4, pp. 235-238, April 1976.
- [41] V. Rizzoli and A. Lipparini, “Computer-aided noise analysis of linear multiport networks of arbitrary topology,” *IEEE Trans. Microwave Theory and Techniques*, vol. MTT-33, no. 12, pp. 1507-1512, December 1985.
- [42] M. E. Mokari and W. Patience, “ A new method of noise parameter calculation using direct matrix analysis,” *IEEE Trans. Circuits and Systems – I: Fundamental Theory and Applications*, vol. 39, no. 9, pp. 767-771 , September 1992.
- [43] C. H. Chen and M. J. Deen, “Direct calculation of the MOSFET high frequency noise parameters,” *Journal of Vacuum Science and Technology A*, vol. 16(2), pp. 850 - 854, March/April 1998.
- [44] C. H. Chen and M. J. Deen, “High frequency noise of MOSFETs I - modeling,” *Solid-State Electronics*, vol. 42(11), pp. 2069 - 2081, November 1998.

- [45] N. J. Kuhn, "Curing a subtle but significant cause of noise figure error," *Microwave J.*, pp. 85-98, June 1984.
- [46] M. W. Medley, *Microwave and R Circuits: Analysis, Synthesis and Design*, Artech House, Inc., 1993.
- [47] V. Adamian and A. Uhler, "Simplified noise evaluation of microwave receivers," *IEEE Trans. Instrumentation and Measurement*, vol. IM-33, no. 2, pp. 136-140, June 1984.
- [48] L. Escottee, R. Plana and J. Graffeuil, "Evaluation of noise parameter extraction methods," *IEEE Trans. Microwave Theory Tech.*, vol. 41, no. 3, pp. 382-387, March 1993.
- [49] *Focus Microwave, Tuner Operation Basics*. Available: <http://focus-microwaves.com/template.php?unique=157>.
- [50] *Maury Microwave, Microwave Tuners*. Available : <http://www.microwaves101.com/encyclopedia/tuners.cfm>.
- [51] *Agilent Noise Source Calibration*, Product Note 5988-7229EN.
- [52] *Noise Figure Measurement Accuracy*, Application Note 57-2.
- [53] *Practical Noise-Figure Measurement and Analysis for Low-Noise Amplifier Designs*, Application Note 1354.

Appendix A

Scattering Parameters

This section will discuss the concepts and definitions to scattering parameters and how it applies to device characterization. The s-parameter matrix is the standard method used for device characterization at radio frequencies. When a propagating waveform travels along a transmission line and through a device under test, s-parameters can be defined as functions of the incident, reflected and transmitted waveforms (see Figure A-1). The incoming wave on the transmission line consists of an amplitude and phase. The s-parameters describe the flow of energy and the relation of the network to the DUT. For a 2 port network the s-parameters can be conceptually thought as the following:

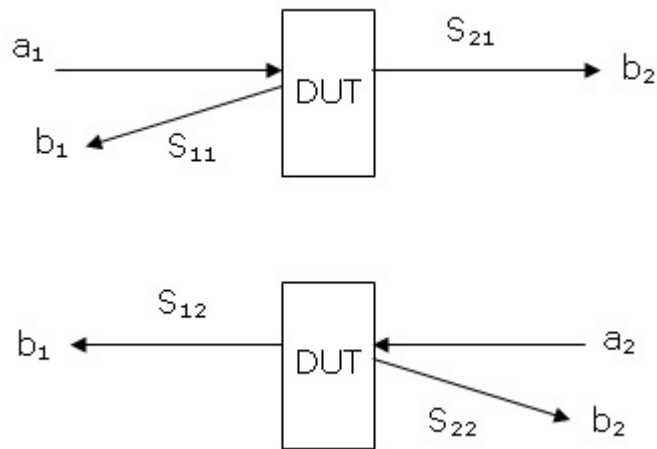


Figure A-1: S-Parameter Signal Flow Diagram.

S_{11} is related the reflected wave when a signal travels into port 1

S_{12} is related the transmitted wave when a signal travels through port 1 to port 2

S_{22} is related the reflected wave when a signal travels into port 2

S_{21} is related the transmitted wave when a signal travels through port 2 to port 1

S-parameters are the reflection and transmission parameters of a network and relate to travelling normalized voltage waves. It can be expressed as a normalized incident and reflected wave travelling into a port n (n represents any port within a network) as,

$$a_n = \frac{V_n^+}{\sqrt{Z_{0n}}}, \quad (\text{A.1})$$

$$b_n = \frac{V_n^-}{\sqrt{Z_{0n}}}. \quad (\text{A.2})$$

The normalized waves (a_n and b_n) are measured at the reference plane of each port, which in most cases is the ends of a coaxial connector or a probe tip. They also can directly relate to power as the forward and reverse voltage waves are normalized to an impedance.

The s-parameters can also be represented in matrix form and for a 2 port network (see Figure A-2) the matrix can be expressed as,

$$\begin{bmatrix} b_1 \\ b_2 \end{bmatrix} = \begin{bmatrix} S_{11} & S_{12} \\ S_{21} & S_{22} \end{bmatrix} \begin{bmatrix} a_1 \\ a_2 \end{bmatrix}$$

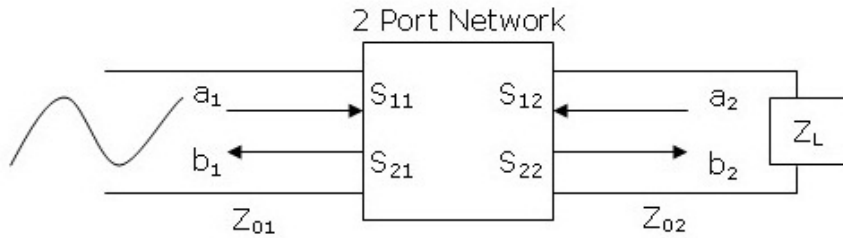


Figure A-2: S-Parameter 2 Port Network.

Expanding the matrix gives the following expressions,

$$b_1 = S_{11}a_1 + S_{12}a_2, \quad (\text{A.3})$$

$$b_2 = S_{22}a_2 + S_{21}a_1. \quad (\text{A.4})$$

Using (A.2) and (A.3), a general s-parameter definition can be derived when one port is terminated with a matched load (see Figure A-3) as,

$$S_{ij} = \left. \frac{b_j}{a_i} \right|_{a_k=0 \text{ for all } k \neq j} \quad (\text{A.5})$$

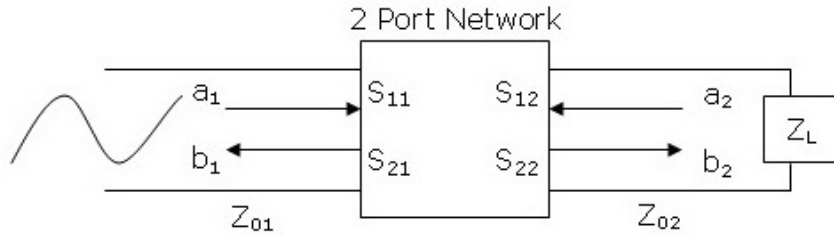


Figure A-3: S-Parameter 2 Port Network with Load Impedance.

This general definition only applies under the condition that there is no signal at any port other than j. This condition is met when all other ports (e.g. port i) is terminated with a matched load ($Z_{01} = Z_{02}$). For Example,

$$S_{21} = \frac{b_2}{a_1} = \frac{V_2^-}{\sqrt{Z_{02}}} \frac{\sqrt{Z_{01}}}{V_1^+}, \quad (\text{A.6})$$

$$S_{21} = \frac{V_2^-}{V_1^+} \text{ when } Z_{01} = Z_{02}. \quad (\text{A.7})$$

This shows that S_{21} is a ratio of the incident voltage at port 1 to the output voltage at port 2 and in general, under a matched condition, s-parameters can be simply expressed as a ratio of voltages.

S-parameters can also be related to the total voltages and currents, enabling small signal analysis. From Figure A-4, the following equations can be derived for a 2 port network,

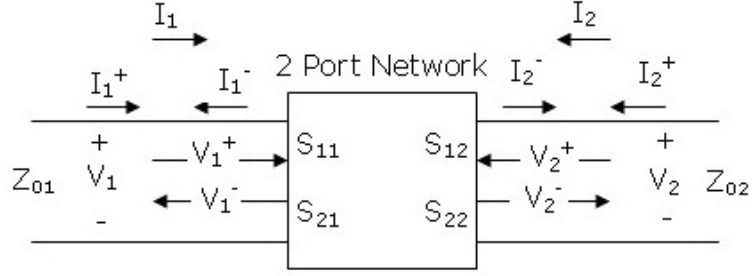


Figure A-4: S-Parameter 2 Port Network with Total Voltage and Current.

$$V_1 = V_1^+ + V_1^-, \quad (\text{A.8})$$

$$I_1 = \frac{V_1^+ - V_1^-}{Z_{01}}, \quad (\text{A.9})$$

$$V_2 = V_2^+ + V_2^-, \quad (\text{A.10})$$

$$I_2 = \frac{V_2^+ - V_2^-}{Z_{02}}. \quad (\text{A.11})$$

Using (A.6)-(A.11), another general definition can be easily derived as,

$$S_{ij} = \frac{V_i - I_i Z_{0i}}{V_j - I_j Z_{0j}}. \quad (\text{A.12})$$

By applying both general definitions (A.5) and (A.12) and assuming a fully matched 2 port network as shown in Figure A-5, the s-parameters for practical purposes can be defined as,

S_{11} is the forward reflection coefficient (input return loss) when the output port is terminated in a matched load and is expressed by,

$$S_{11} = \left. \frac{b_1}{a_1} \right|_{a_2=0} = \Gamma_{in1} \Big|_{a_2=0} = \frac{Z_{in1} - Z_{01}}{Z_{in1} + Z_{01}}. \quad (\text{A.13})$$

S_{22} is the reverse reflection coefficient (output match) and is expressed by,

$$S_{22} = \left. \frac{b_2}{a_2} \right|_{a_1=0} = \Gamma_{in2} \Big|_{a_1=0} = \frac{Z_{in2} - Z_{02}}{Z_{in2} + Z_{02}}. \quad (\text{A.14})$$

S_{21} is the forward transmission coefficient (forward gain or insertion loss) and is expressed by,

$$S_{21} = \left. \frac{b_2}{a_1} \right|_{a_2=0} = \frac{V_2 - I_2 Z_{02}}{V_1 - I_1 Z_{01}} = \frac{2V_2}{V_s}, \quad (\text{A.15})$$

since $-I_2 Z_{02} = V_2$ and $V_1 + I_1 Z_{01} = V_s$

S_{12} is the reverse transmission coefficient (isolation) and is expressed by,

$$S_{12} = \left. \frac{b_1}{a_2} \right|_{a_1=0} = \frac{2V_1}{V_s}. \quad (\text{A.16})$$

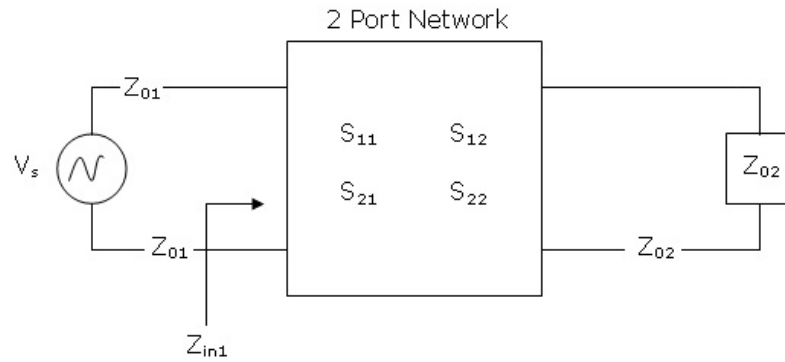


Figure A-5: S-Parameter Complete 2 Port Network.

Appendix B

Network Analyzer: Error Correction Model

The network analyzer is a common instrument used for measurement at radio frequencies as it can report scattering parameters for devices under test. As discussed in previous sections, there are major advantages to device characterization using s-parameters. However, to accurately report measurement data, it is necessary for the network analyzer to be calibrated. The calibration process is intended to remove systematic errors presented by the instrument and connectors. This appendix will discuss and derive the full 2 port error model.

Error Correction Model

Full 2 port calibration (SOLT) consists of 12 error terms. Each error term represents a systematic error within the network (see Table B-1 and Table B-2) by following the calibration procedure, all 12 terms will be determined and can be used for future measurement when the PNA is set to correction mode. The following section will discuss how the PNA internally solves for each error term and determines the actual s-parameters of the DUT. Figure B-1 and B-2, shows that the errors can be thought of as one block between a perfect reflectometer and the DUT. For full 2 port calibration, it involves 3 major steps:

1. One Port (S_{11} and S_{22}) Calibration
2. Isolation
3. Transmission

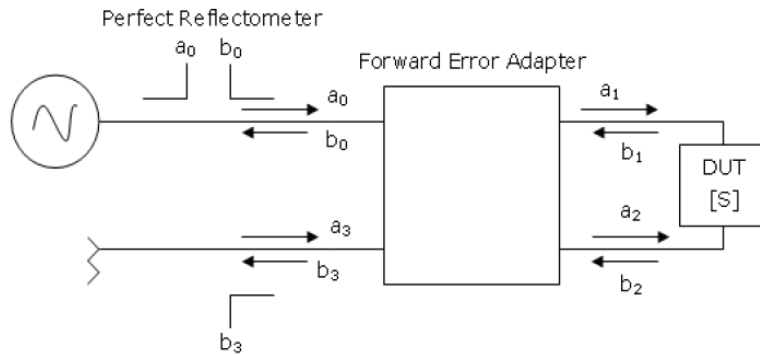


Figure B-1: Forward Error Model [16].

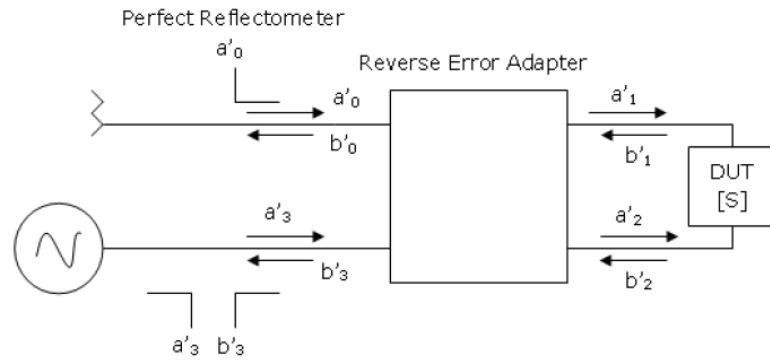


Figure B-2: Reverse Error Model [16].

Table B-1: Forward Transmission Error Terms.

e_{00}	Directivity
e_{11}	Port 1 Match
$(e_{10}e_{01})$	Reflection Tracking
$(e_{10}e_{32})$	Transmission Tracking
e_{22}	Port 2 Match
e_{30}	Leakage

Table B-2: Reverse Transmission Error Terms.

e'_{33}	Directivity
e'_{11}	Port 1 Match
$(e'_{23}e'_{32})$	Reflection Tracking
$(e'_{23}e'_{01})$	Transmission Tracking
e'_{22}	Port 2 Match
e'_{03}	Leakage

First we consider the complete error term model for forward and reverse model as shown in Figure B-3 and Figure B-4 respectively. The s-parameters of the DUT are embedded in the signal flow model and in order to determine the actual s-parameters of the DUT, we need to determine the relationship of the measured s-parameters, the s-parameters of the DUT and the error terms.

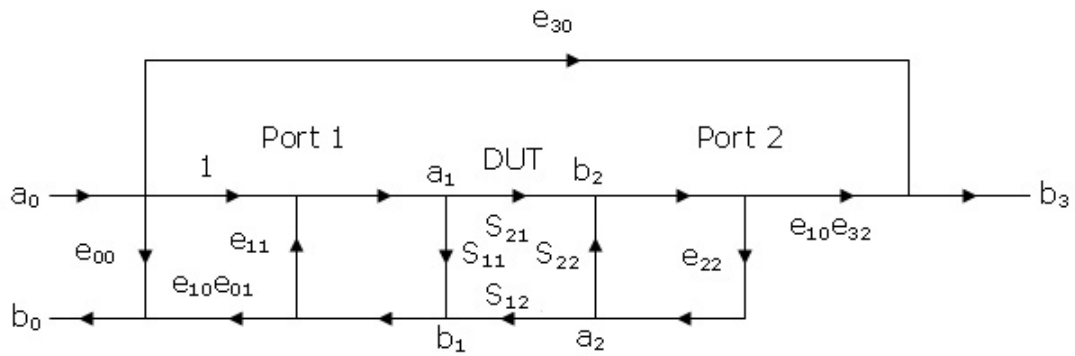


Figure B-3: Complete Forward Error Signal Flow [16].

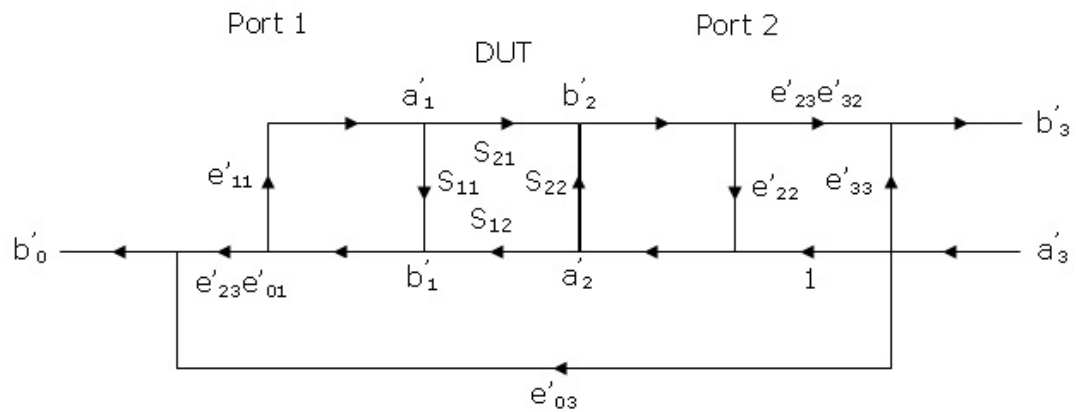


Figure B-4: Complete Reverse Error Signal Flow [16].

To calculate S_{11M} , S_{21M} , S_{12M} and S_{22M} , we utilize the following rules when simplifying the signal flow diagram.



Figure B-5: Series Rule.

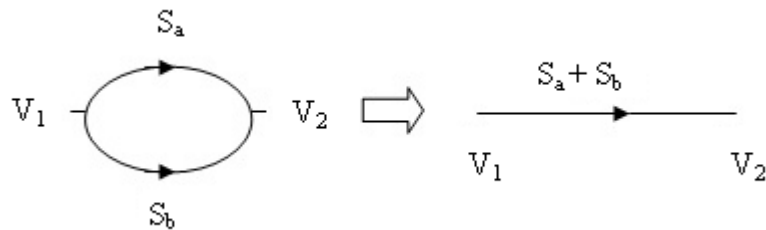


Figure B-6: Parallel Rule.

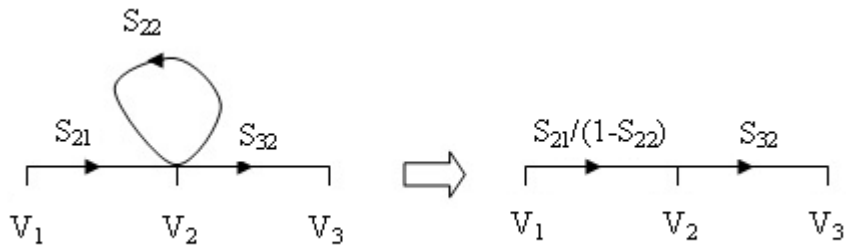


Figure B-7: Self Loop Rule.

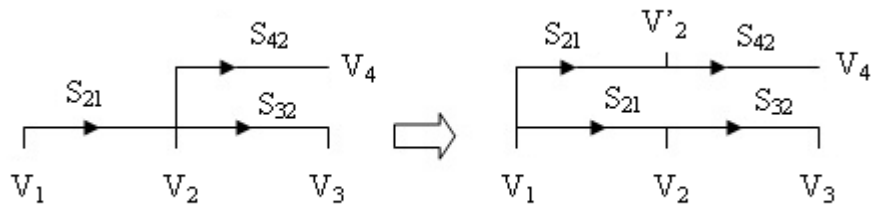


Figure B-8: Splitting Rule.

To solve S_{11M} and S_{21M} , we begin with the complete forward model,

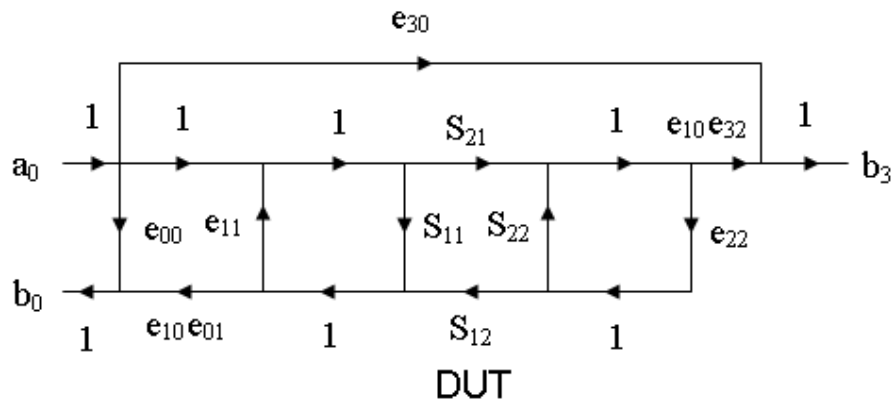


Figure B-9: Complete Forward Model.

By applying the series rule we get,

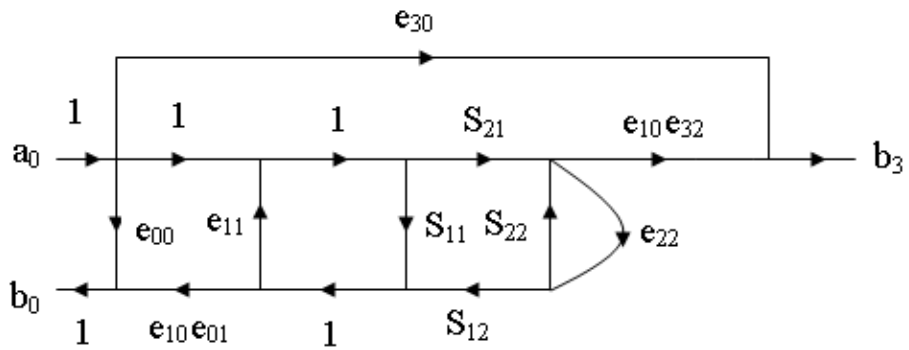


Figure B-10: Error Model simplification after applying series rule.

Now applying the series rule we get,

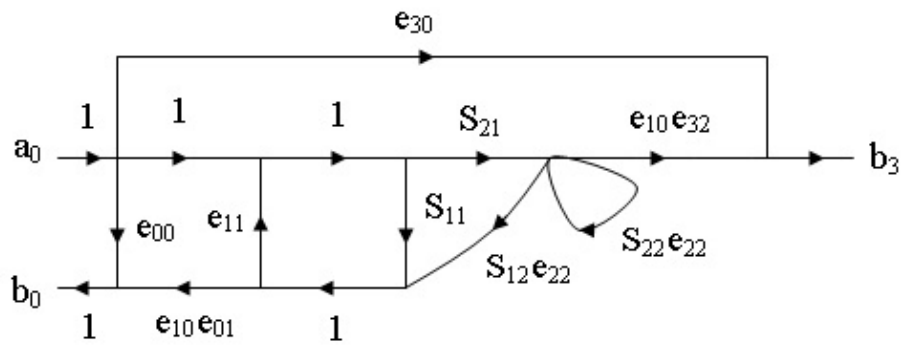


Figure B-11: Error Model simplification after applying series rule.

Now applying the self loop rule we get,

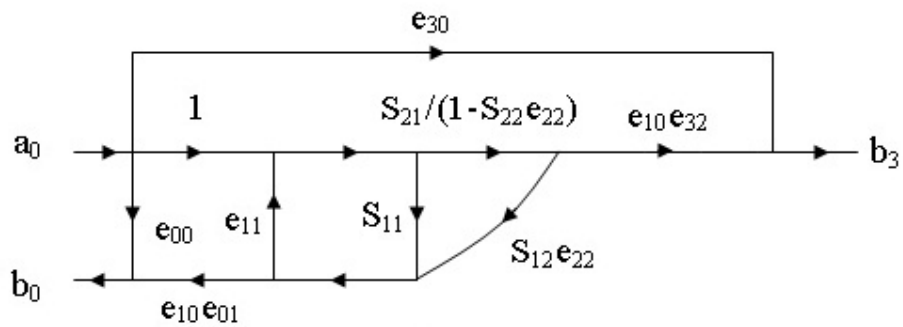


Figure B-12: Error Model simplification after applying self loop rule.

Now applying the series rule we get,

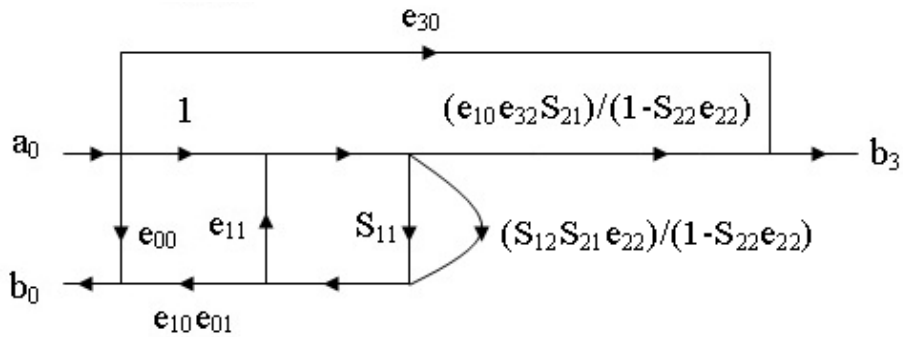


Figure B-13: Error Model simplification after applying series rule.

Now applying the parallel rule we get,

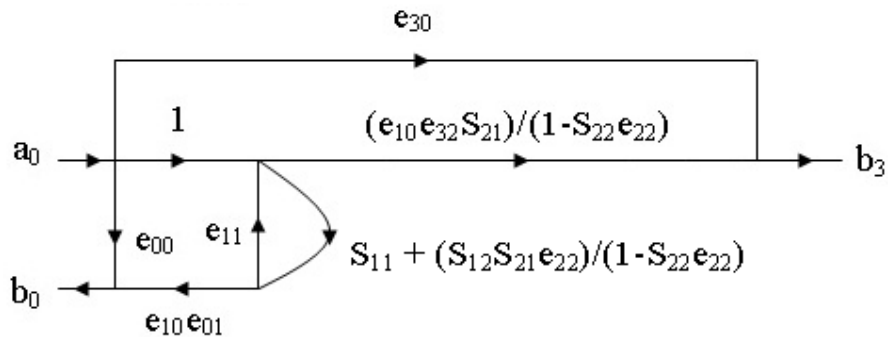


Figure B-14: Error Model simplification after applying parallel rule.

Now applying the series rule we get,

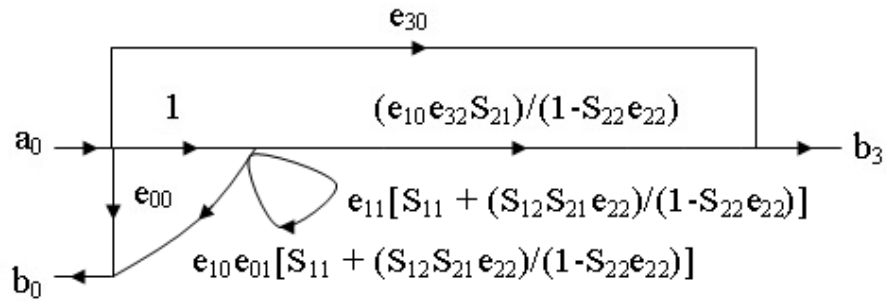


Figure B-15: Error Model simplification after applying series rule.

Now applying the self loop rule we get,

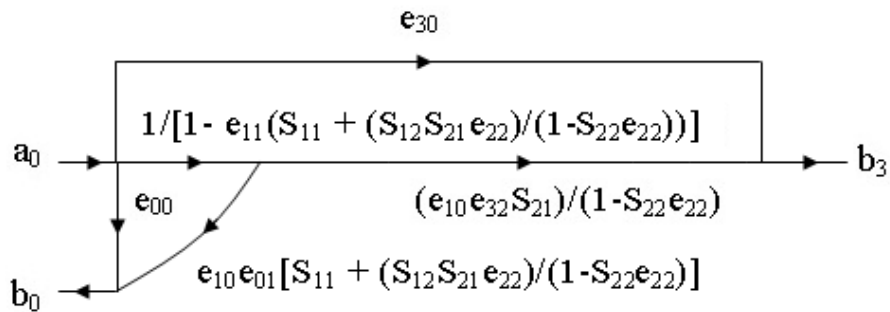


Figure B-16: Error Model simplification after applying self loop rule.

Now applying the series rule we get,

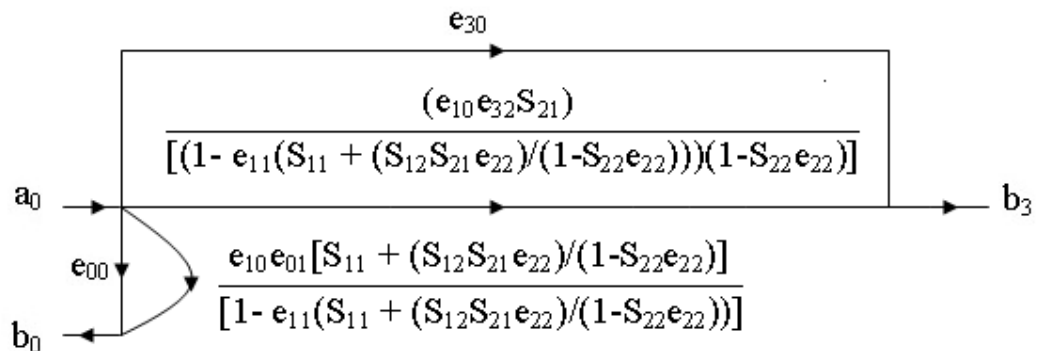


Figure B-17: Error Model simplification after applying series rule.

Finally, applying the self loop rule we get S_{11M} and S_{21M} .

$$\begin{array}{c}
 \begin{array}{ccc}
 & \xrightarrow{\quad \quad \quad} & \\
 a_0 & \xrightarrow{\quad \quad \quad} & b_3 \\
 \downarrow & & \\
 b_0 & &
 \end{array} \\
 e_{30} + \frac{(e_{10}e_{32}S_{21})}{[(1 - e_{11}(S_{11} + (S_{12}S_{21}e_{22})/(1 - S_{22}e_{22}))) (1 - S_{22}e_{22})]} = S_{21M} \\
 e_{00} + \frac{e_{10}e_{01}[S_{11} + (S_{12}S_{21}e_{22})/(1 - S_{22}e_{22})]}{[1 - e_{11}(S_{11} + (S_{12}S_{21}e_{22})/(1 - S_{22}e_{22}))]} = S_{11M}
 \end{array}$$

Figure B-18: S_{11M} and S_{21M} solution after applying self loop rule.

A similar exercise can be performed to determine S_{12M} and S_{22M} .

One Port Calibration

The first step will be the forward one port model. This process will extract e_{00} , e_{11} , ($e_{10}e_{01}$) via S_{11} measurement. The signal flow model is shown in Figure B-19.

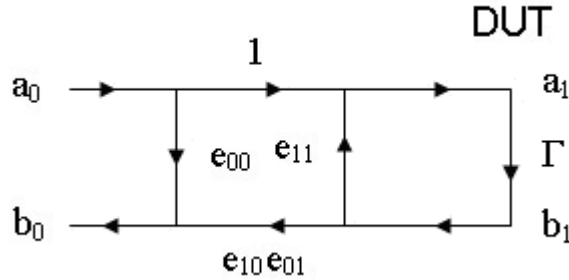


Figure B-19: One Port Error Signal Flow.

Using nodal analysis at a_0 , a_1 , b_0 and b_1 , the following equations can be derived,

$$a_1 = a_0 + e_{11}b_1, \tag{B.1}$$

$$b_0 = e_{00}a_0 + e_{10}e_{01}b_1, \tag{B.2}$$

$$b_1 = a_1\Gamma. \tag{B.3}$$

It is known that the general s-parameter definition is $S_{11} = \Gamma = \frac{b_1}{a_1}$ therefore by applying the

above the following equation can be determined.

$$\Gamma_{Measured} = \frac{b_0}{a_0} = e_{00} + e_{10}e_{01} \frac{b_1}{a_0} = e_{00} + e_{10}e_{01} \frac{b_1}{a_1 - (e_{11}\Gamma)} = e_{00} + \frac{e_{10}e_{01}\Gamma}{1 - e_{11}\Gamma} = \frac{e_{00}\Delta_e\Gamma}{1 - e_{11}\Gamma}, \quad (\text{B.4})$$

where

$$\Delta_e = e_{00}e_{11} - (e_{10}e_{01})$$

$\Gamma_{Measured}$ is the measured reflection coefficient from the PNA

and

Γ is the actual reflection coefficient of the measured device or DUT.

Three $\Gamma_{Measured}$ are determined by connecting the calibration standards (open, short, load) to each port. Theoretically, $\Gamma = 1$ (full reflection) for calibration standards open and short and $\Gamma = 0$ (no reflection) for a load. By re-arranging the above equation, we can derive the following for each known standard.

$$e_{00} + \Gamma_{short} \Gamma_{measured1} e_{11} - \Gamma_{short} \Delta_e = \Gamma_{measured1} \quad (\text{B.5})$$

$$e_{00} + \Gamma_{open} \Gamma_{measured2} e_{11} - \Gamma_{open} \Delta_e = \Gamma_{measured2} \quad (\text{B.6})$$

$$e_{00} + \Gamma_{load} \Gamma_{measured3} e_{11} - \Gamma_{load} \Delta_e = \Gamma_{measured3} \quad (\text{B.7})$$

Similar analysis can be performed to determine the reverse transmission error terms (e'_{33} , e'_{22} and ($e'_{23}e'_{32}$)) for the second port. The errors terms can now be solved using linear algebra (3 equations, 3 unknowns). Each error term can be modeled in matrix form and can be thought of as s-parameters. Therefore, we can represent the forward and reverse error terms as,

$$\begin{bmatrix} e_{00} & 1 \\ e_{10}e_{01} & e_{11} \end{bmatrix} = \begin{bmatrix} e_{00} & e_{01} \\ e_{10} & e_{11} \end{bmatrix}, \quad (\text{B.8})$$

$$\begin{bmatrix} e'_{33} & 1 \\ e'_{23}e'_{32} & e'_{22} \end{bmatrix} = \begin{bmatrix} e'_{33} & e'_{32} \\ e'_{23} & e'_{22} \end{bmatrix}. \quad (\text{B.9})$$

Isolation

To extract e_{30} and e'_{03} , we connect the load standard ($S_{12} = S_{21} = 0$) to each port and measure S_{21} for forward leakage and S_{12} for reverse leakage.

Transmission

To extract the remaining four terms, e_{22} and $e_{10}e_{32}$ for forward model and e'_{11} and $e'_{23}e'_{01}$ for reverse model, we connect the port 1 and 2 with a thru ($S_{11} = S_{22} = 0$ and $S_{12} = S_{21} = 1$). Following the same nodal analysis and measuring S_{11} and S_{21} for the forward model yields,

$$e_{22} = \frac{S_{11M} - e_{00}}{S_{11M}e_{11} - \Delta_e} \quad (\text{B.8})$$

$$e_{10}e_{32} = (S_{21M} - e_{30})(1 - e_{11}e_{22}) \quad (\text{B.9})$$

Measuring S_{22} and S_{12} for the reverse model yields,

$$e'_{11} = \frac{S_{22M} - e'_{33}}{S_{22M}e'_{22} - \Delta_e} \quad (\text{B.10})$$

$$e'_{23}e'_{01} = (S_{12M} - e'_{03})(1 - e'_{11}e'_{22}) \quad (\text{B.11})$$

After all 12 error terms are known, calibration is complete and the PNA simultaneously solves the measured s-parameter equations to report the actual s-parameters of the DUT. We can also rearrange the equations to show the s-parameters of the DUT as,

$$S_{11} = \frac{\left(\frac{S_{11M} - e_{00}}{e_{10}e_{01}} \right) \left(1 + \frac{S_{22M} - e'_{33}}{e'_{23}e'_{32}} e'_{22} \right) - e_{22} \left(\frac{S_{21M} - e_{30}}{e_{10}e_{32}} \right) \left(\frac{S_{21M} - e'_{03}}{e'_{23}e'_{01}} \right)}{D} \quad (\text{B.12})$$

$$S_{21} = \frac{\left(\frac{S_{21M} - e_{30}}{e_{10}e_{32}} \right) \left(1 + \frac{S_{22M} - e'_{33}}{e'_{23}e'_{32}} (e'_{22} - e_{22}) \right)}{D} \quad (\text{B.13})$$

$$S_{22} = \frac{\left(\frac{S_{22M} - e'_{33}}{e'_{23}e'_{32}} \right) \left(1 + \frac{S_{11M} - e_{00}}{e_{10}e_{01}} e_{11} \right) - e'_{11} \left(\frac{S_{21M} - e_{30}}{e_{10}e_{32}} \right) \left(\frac{S_{21M} - e'_{03}}{e'_{23}e'_{01}} \right)}{D} \quad (\text{B.14})$$

$$S_{12} = \frac{\left(\frac{S_{12M} - e'_{03}}{e'_{23}e'_{01}} \right) \left(1 + \frac{S_{11M} - e_{00}}{e_{10}e_{01}} (e_{11} - e'_{11}) \right)}{D} \quad (\text{B.15})$$

where $D = \left(1 + \frac{S_{11M} - e_{00}}{e_{10}e_{01}} e_{11} \right) \left(1 + \frac{S_{22M} - e'_{33}}{e'_{23}e'_{32}} e'_{22} \right) - \left(\frac{S_{21M} - e_{30}}{e_{10}e_{32}} \right) \left(\frac{S_{12M} - e'_{03}}{e'_{23}e'_{01}} \right) e_{22}e'_{11}$.

Appendix C

S Domain to ABCD Domain Conversion Table

$$A' = \frac{(1 + S_{11})(1 - S_{22}) + S_{12}S_{21}}{2S_{21}} \quad (\text{D.1})$$

$$B' = \frac{(1 + S_{11})(1 + S_{22}) - S_{12}S_{21}}{2S_{21}} \quad (\text{D.2})$$

$$C' = \frac{(1 - S_{11})(1 - S_{22}) - S_{12}S_{21}}{2S_{21}} \quad (\text{D.3})$$

$$D' = \frac{(1 - S_{11})(1 + S_{22}) + S_{12}S_{21}}{2S_{21}} \quad (\text{D.4})$$

$$\text{where } \begin{cases} A = A' \\ B = Z_0 B' \\ C = \frac{C'}{Z_0} \\ D = D' \end{cases} .$$

$$S_{11} = \frac{A'+B'-C'-D'}{\Delta} \quad (\text{D.5})$$

$$S_{12} = \frac{2(A'D'-B'C')}{\Delta} \quad (\text{D.6})$$

$$S_{21} = \frac{2}{\Delta} \quad (\text{D.7})$$

$$S_{22} = \frac{-A'+B'-C'+D'}{\Delta} \quad (\text{D.8})$$

$$\text{where } \begin{cases} A = A' \\ B = Z_0 B' \\ C = \frac{C'}{Z_0} \\ D = D' \end{cases} \quad \text{and } \Delta = A'+B'+C'+D' \quad .$$

Appendix D

Software Operations Manual

This section describes in detail the step by step operation of the newly developed noise measurement system. Figure D-1 shows the user interface of the system.

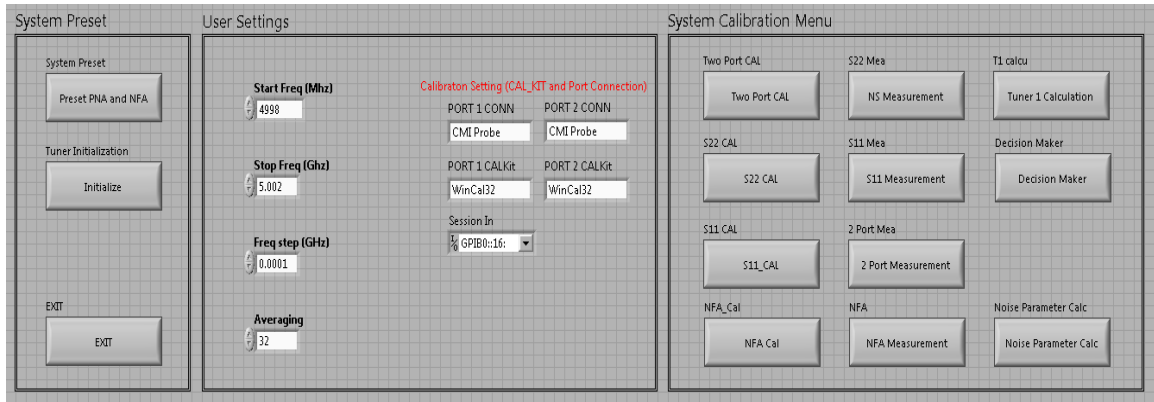


Figure D-1: Software System User Interface.

Step 1- System Initialization

- Create a 'DATA' folder in the same location where the program was launched. Note: All data files will be saved into this directory and make necessary hard code changes for custom frequency settings to ensure correct data points are measured and ENR file location is valid.
- Click the forward arrow button to execute the software program.
- Click 'Preset PNA and NFA' and wait for response. This button will put the PNA and NFA into default mode.
- Click 'Initialize' and wait for response. This button will initial the tuners to its default position.

- Click 'Exit.' This button will end the current session.
- Key in the desired Start/Stop Frequency, Frequency Step and Averaging values.

Step 2 – Perform full two port calibration

- Click 'Two Port CAL.' This button will begin the SOLT calibration sequence. You will be asked to perform the calibration offline.
- On the PNA, go to Calibration and select Calibration Wizard.
- Follow the instructions and select '2 port solt' with 'WinCal32' Cal Kit.
- Continue on and probe the corresponding short, open, load and thru standards on the calibration substrate and click 'Finish' on the PNA and click 'OK' in Labview.
- Labview will save the calibration all 12 error terms in files: DIR(11).txt, SM(11).txt, RT(11).txt, CT(12).txt, TT(12).txt, LM(12).txt, DIR(22).txt, SM(22).txt, RT(22).txt, TT(21).txt and LM(21).txt.
- Click '2 Port Measurement' and wait for response. This button will first measure the s-parameters of the on-wafer device and save the files: S11_Thru.txt, S12_Thru.txt, S21_Thru.txt and S22_Thru.txt. Then the program will determine the Γ_{inr} of the receiver at the receiver reference plane and save the file: gamma_inr.txt.

Step 3 – S₂₂ Calibration

- Replace the noise source with the ECAL module and click 'S22 Cal' and wait for response. This button will perform one port calibration and save all the one port error terms in files: S22_DIR.txt, S22_RT.txt and S22_SM.txt.

- Connect the noise source back and click ‘NS Measurement.’ This button will measure the S_{22} at source tuner reference plane for a hot and cold noise source and save the files: NS_S22_hot.txt and NS_S22_cold.txt.

Step 4 – Source Tuner Characterization

- Create two text files named ‘Source Tuner Position Low Band.txt’ and ‘Source Tuner Position High Band.txt’ in the DATA folder. In these files, list all the tuner positions that will be used for tuner characterization.
- Replace the noise source with the ECAL module and click ‘Tuner 1 Calculation.’ This button will determine the source tuner s-parameter data at all positions listed in the above files for low and high band. The one port error terms and the tuner s-parameters will be saved in the following format for all positions listed:
 - S22_Low_(error_term)_(position).txt and S22_High_(error_term)_(position).txt
 - S11_T_Low_(position).txt, S12_T_Low_(position).txt,
S21_T_Low_(position).txt and S22_T_Low_(position).txt
 - S11_T_High_(position).txt, S12_T_High_(position).txt,
S21_T_High_(position).txt and S22_T_High_(position).txt

Step 5 – Noise Power Measurement

- Create two text files named ‘Noise Position Low Band.txt’ and ‘Noise Position High Band.txt’ into the DATA folder. These files can be the same or a subset of the source tuner position files.

- Re-connect the noise source and click ‘NFA Measurement.’ This button will measure the hot and cold noise power at all positions listed and save the measurements in the following format for all positions listed:
 - PCOLD_Low_(position).txt and PHOT_Low_(position).txt,
 - PCOLD_High_(position).txt and PHOT_High_(position).txt.

Step 6 – Data Output for Noise Parameter Extraction

- Click ‘Noise Parameter Calc.’ This button will create Low and High Band Output.txt files that contain all measurement data and create noise data files for noise parameter extraction in MATLAB.

Step 7 – Noise Parameter Extraction in MATLAB

- Open the file ‘NoiseParamExtract.m’ and modify as necessary and run.
- Noise parameters will be saved in tables: NF_{min} , R_n , G_{opt} and B_{opt} .